Original Article

MOLECULAR METABOLISM

Exercise-induced specialized proresolving mediators stimulate AMPK phosphorylation to promote mitochondrial respiration in macrophages

Ernesto Pena Calderin [1,2], Jing-Juan Zheng [1], Nolan L. Boyd [1], Lindsey McNally [1], Timothy N. Audam [1], Pawel Lorkiewicz [1], Bradford G. Hill [1], Jason Hellmann [1,*]

ABSTRACT

Objective: Physical activity has been shown to reduce the risk of CVD mortality in large-cohort longitudinal studies; however, the mechanisms underpinning the beneficial effects of exercise remain incompletely understood. Emerging data suggest that the risk reducing effect of exercise extends beyond changes in traditional CVD risk factors alone and involves alterations in immunity and reductions in inflammatory mediator production. Our study aimed to determine whether exercise-enhanced production of proresolving lipid mediators contribute to alterations in macrophage intermediary metabolism, which may contribute to the anti-inflammatory effects of exercise.

Methods: Changes in lipid mediators and macrophage metabolism were assessed in C57Bl/6 mice following 4 weeks of voluntary exercise training. To investigate whether exercise-stimulated upregulation of specialized proresolving lipid mediators (SPMs) was sufficient to enhance mitochondrial respiration, both macrophages from control mice and human donors were incubated *in vitro* with SPMs and mitochondrial respiratory parameters were measured using extracellular flux analysis. Compound-C, an ATP-competitive inhibitor of AMPK kinase activity, was used to investigate the role of AMPK activity in SPM-induced mitochondrial metabolism. To assess the *in vivo* contribution of 5-lipoxygenase in AMPK activation and exercise-induced mitochondrial metabolism in macrophages, *Alox5*$^{-/-}$ mice were also subjected to exercise training.

Results: Four weeks of exercise training enhanced proresolving lipid mediator production, while also stimulating the catabolism of inflammatory lipid mediators (e.g., leukotrienes and prostaglandins). This shift in lipid mediator balance following exercise was associated with increased macrophage mitochondrial metabolism. We also find that treating human and murine macrophages *in vitro* with proresolving lipid mediators enhances mitochondrial respiratory parameters. The proresolving lipid mediators RvD1, RvE1, and MaR1, but not RvD2, stimulated mitochondrial respiration through an AMPK-dependent signaling mechanism. Additionally, in a subset of macrophages, exercise-induced mitochondrial activity *in vivo* was dependent upon 5-lipoxygenase activity.

Conclusion: Collectively, these results suggest that exercise stimulates proresolving lipid mediator biosynthesis and mitochondrial metabolism in macrophages via AMPK, which might contribute to the anti-inflammatory and CVD risk reducing effect of exercise.

Keywords Exercise; Macrophage; Inflammation; Mitochondria; Lipid mediators

1. INTRODUCTION

Exercise decreases morbidity and all-cause mortality in large part by protecting against the development and progression of cardiovascular disease. After controlling for changes in traditional cardiovascular risk factors such as lipids (e.g., low density lipoprotein), body weight, and blood pressure, reductions in inflammatory factors contribute significantly to the cardiovascular risk reducing effect of exercise [1–3]. Nevertheless, the cellular mechanisms responsible for the beneficial effects of exercise remain incompletely understood. We have recently reported that the anti-inflammatory response to exercise is modified by plasma levels of omega-3 polyunsaturated fatty acids and that exercise enhances the production of omega-3 polyunsaturated fatty acid-derived specialized proresolving mediators (SPMs), which stimulate macrophage phagocytosis and resolution of acute inflammation [4,5]. Macrophage function and metabolism are interconnected. Anti-inflammatory M2 macrophages that are responsible for tissue repair and homeostasis rely primarily on the TCA cycle and oxidative phosphorylation for the generation of ATP with less dependence on ATP derived from glycolysis [6–10]. Conversely, classically activated M1

[1]Diabetes and Obesity Center, Christina Lee Brown Envirome Institute, Division of Environmental Medicine, University of Louisville School of Medicine, Louisville, KY, 40202, USA [2]Department of Physiology, University of Louisville School of Medicine, Louisville, KY, 40202, USA

*Corresponding author. 580 S. Preston St. Rm 204F, Delia Baxter II Building, University of Louisville, Louisville, KY 40202, USA. E-mail: Jason.hellmann@louisville.edu (J. Hellmann).

Received October 21, 2022 • Accepted November 7, 2022 • Available online 15 November 2022

Abbreviations

CVD	cardiovascular disease
SPM	specialized proresolving mediators
RvD1	Resolvin D1
RvD2	Resolvin D2
RvE1	Resolvin E1
MaR1	Maresin 1
IRG1	immune response gene 1
hPBMC	human peripheral blood mononuclear cells
hMDM	human monocyte-derived macrophages
M-CSF	macrophage colony-stimulating factor
GM-CSF	granulocyte macrophage colony-stimulating factor
BMDM	bone-marrow-derived macrophages
CompC	compound C
OCR	oxygen consumption rate
FcR	Fc receptor
XF	extracellular flux
PLS-DA	Partial Least-squares Discriminate Analysis
$\Delta\Psi m$	mitochondrial membrane potential
MFI	mean fluorescence intensity
CLSM	confocal laser scanning microscopy
5-LO	5-lipoxygenase
Alox5	5-lipoxygenase-coding gene
LTB_4	leukotriene B4
PGD_2	prostaglandin D2
PGE_2	prostaglandin E2
TXB_2	thromboxane B2
NC	necroptotic cells
iNOS	inducible nitric oxide synthase
ARG1	arginase 1
LM	lipid mediator
TP	prostanoids TP receptor
AnxA1	annexin A1
CaMK	Ca^{2+}/calmodulin-dependent protein kinase
ACC	Acetyl-CoA carboxylase
LPS	lipopolysaccharides
FFA	free fatty acids
CPT1	carnitine palmitoyl transferase 1
HFD	high fat diet
MCP-1	Monocyte Chemoattractant Protein 1

inflammatory macrophages derive ATP primarily through substrate-level phosphorylation via upregulation of key glycolytic isozymes, which are also directly involved in the upregulated secretion of proinflammatory cytokines IL-1β, IL-6, and TNFα [11–16]. Inflammatory murine M1 macrophages display an interrupted TCA cycle resulting in the accumulation of citrate and succinate [17,18]. Citrate accumulation drives acetyl CoA production and increases fatty acid synthase activity, resulting in the upregulation of *de novo* proinflammatory lipid (i.e., prostaglandins) biosynthesis [19], while accumulated succinate serves as a pseudohypoxia response sensor by stabilizing HIF1-α and inducing IL-1β production [18,20,21]. Additionally, upregulation of glycolytic flux feeds the pentose phosphate pathway, which in addition to supplying amino acids and nucleotides to satisfy the biosynthetic needs of the highly secretory phenotype of M1 macrophages, increases NADPH-driven reactive oxygen species (ROS) formation and NO production [22]. ROS formation further drives HIF-1α-dependent IL-1β secretion, while NO, along with citrate-derived (IRG1) itaconate further increases reverse electron transport through ETC complex I, further increasing ROS production in a feedforward cycle [7,21–23]. Despite these significant immunometabolic advances, the role of metabolic intermediates in anti-inflammatory macrophages following exercise are largely unknown.

Emerging evidence suggests that imbalanced proinflammatory to proresolving lipid mediator production contributes to the progression of atherosclerotic cardiovascular disease [24–26]. Specialized proresolving mediators (SPMs) are largely formed by lipoxygenase-derived conversion of omega-3 polyunsaturated fatty acids and are agonists of inflammation-resolution through their actions on GPCRs [27–29]. SPMs are temporally produced and signal the termination of inflammation by quelling aberrant inflammatory signaling pathways, decreasing the recruitment of neutrophils to sites of injury, and by stimulating macrophage phagocytosis. Nonetheless, the extent to which exercise and SPMs alter macrophage metabolism to stimulate phagocytic function and the resolution of inflammation remains largely unknown. In this study, we aimed to assess the contribution of SPM signaling pathways to exercise-induced changes in macrophage metabolism.

2. MATERIALS AND METHODS

2.1. Animals and human samples

Male mice 8–12 weeks of age were maintained on normal chow laboratory diet and housed in temperature-controlled environment (21 °C year-round) with a 12:12-h light/dark cycle. Animals were randomly assigned to experimental groups and housed in groups with up to 5 littermates, except for mice subjected to voluntary wheel running, which were single housed for the duration of the exercise protocol. *Fpr2*$^{-/-}$ mice were maintained on a C57BL/6Ntac background as provided by Idorsia Pharmaceuticals and C57BL/6NTac from Taconic Bioscience (Germantown, New York) were bred in-house and served as *Fpr2*$^{-/-}$ controls. *Alox5*$^{-/-}$ (B6.129S2-*Alox5*^{tm1Fun}/J) mice on the C57BL/6J background were purchased from The Jackson Laboratory (strain # 004155) and C57BL/6J mice purchased from The Jackson Laboratory (strain # 000664) served as controls for studies involving *Alox5*$^{-/-}$ mice. Resolvin D1 (RvD1; 7S,8R,17S-trihydroxy-4Z,9E,11E,13Z,15E,19Z-docosahexaenoic acid), Resolvin D2 (RvD2; 7*S*,16*R*,17*S*-trihydroxy-4*Z*,8*E*,10*Z*,12*E*,14*E*,19*Z*-docosahexaenoic acid), Resolvin E1 (RvE1; 5S,12R,18R-trihydroxy-6Z,8E,10E,14Z,16E-eicosapentaenoic acid) and Maresin1 (MaR1; 7R,14S-dihydroxy-4Z,8E,10E,12Z,16Z,19Z-docosahexaenoic acid) were purchased from Cayman Chemical, catalog numbers: 10012554, 10007279, 10007848 and 10878, respectively. Compound C (CAS 866405-64-3) was purchased from EDM Millipore (cat. # 171261-1 MG). Oligomycin-A (PubChem CID 52947716), FCCP (Carbonyl cyanide p-trifluoromethoxyphenylhydrazone), Antimycin-A (PubChem CID 6450197) and Rotenone (PubChem CID 6758) were purchased from Millipore Sigma (cat.# 04876-5 MG, C2920-10 MG, A8674-50 MG and R8875-1G, respectively)

2.2. Mouse voluntary wheel running exercise

Mice were single-housed in home cages with free access to in-cage stainless steel running wheels (STARR Life Sciences, Oakmont, PA, USA). The mice were randomly assigned to cages containing free-spinning wheels (exercise group) or locked wheels (sedentary control group) for 4 weeks. Wheels of exercised mice were locked 24 h

prior to euthanasia. All other housing conditions were kept constant as previously described.

2.3. Mouse elicited peritoneal macrophage (PM) extraction and culture

To elicit macrophage recruitment, mice were given a sterile 3 mL I.P. injection of 3% w/v brewer modified thioglycolate medium (cat. # 211716, BD, NJ, USA). After 72 h, mice were euthanized and cellular exudates were collected following peritoneal lavage with 3 mL of sterile, room temperature Ca^{2+} Mg^{2+} free DPBS. Cells were enumerated, centrifuged, and supernatant (peritoneal lavage fluid) was collected and stored for further analysis. An aliquot of cells was subjected to Seahorse XFe96 extracellular flux analysis (Agilent Technologies, California, USA) following resuspension in pre-warmed DMEM (cat. # 11-965-092, Thermo Fisher, MA, USA) supplemented with 10% FBS, 100 U/mL penicillin, 100 μg/mL streptomycin, 25 mM D-Glucose and 4 mM L-Glutamine (PM media), while another aliquot was resuspended in Ca^{2+} Mg^{2+} free DPBS with 1% FBS (flow buffer) and subjected to flow cytometric analysis. For the Seahorse XF experiments, 5E4 cells/well were seeded in tissue-culture treated Seahorse XF 96-well culture plates (cat.# 102601-100, Agilent Technologies) and allowed to adhere for 3h at 37 °C, 5% CO_2, in 100 μL PM media per well, before proceeding with the assay.

2.4. Human PBMC isolation and human monocyte-derived macrophage (hMDM) differentiation and culture

Human peripheral blood mononuclear cells (hPBMC) were isolated from fresh mixed, peripheral venous blood by density gradient centrifugation (300 RCF for 10 min) on a 45—50% Percoll gradient (cat.# 17089101, Cytiva Life Sciences, MA, USA). The selection criteria for donors was: healthy male or female; 18—60 years of age; weigh over 110 lb; with no chronic health conditions; and medication-free 24 h prior to blood collection. For *in vitro* differentiation of hPBMC into monocyte-derived macrophages (MDM), 20E6 cells/well were seeded into tissue-culture treated 6-well plates and cultured for 6 days in 3 mL of RPMI1640 (cat.# 21870092, Thermo Fisher) supplemented with 10% heat-shocked fetal bovine serum (FBS) (cat. # S11150H, R&D Systems, MN, USA), 100 U/mL penicillin, 100 μg/mL streptomycin (cat.# P0781-100M, MilliporeSigma, MA, USA), 11.1 mM D-Glucose, 2 mM Glutamax, 1 mM sodium pyruvate (hMDM media), in the presence of either 20 ng/mL human recombinant M-CSF or GM-CSF (cat.# 78057.1 and 78015.1, respectively; STEMCELL Technologies, British Columbia, CA). Cells were washed with DPBS (with Ca^{2+} and Mg^{2+}) and fresh hMDM media added on days 1, 3, 5 and 6 of culture to remove non-adherent cells, metabolic waste, and to provide fresh nutrients. Cells were lifted on day 6 by first washing once with pre-warmed DPBS (Ca^{2+} and Mg^{2+} free) and then by incubating with pre-warmed accutase (cat.# 07922, STEMCELL Technologies) at 37 °C for 5 min, followed by gentle scraping. An aliquot of cells was used for flow cytometric analysis while another for Seahorse XF experiments. For the Seahorse XF experiments, 1.5E5 MDM cells/well were seeded in 300 μL hMDM media in a Seahorse XF 96-well tissue culture treated plate and incubated overnight at 37 °C, 5% CO_2.

2.5. Mouse bone marrow cell isolation and bone marrow-derived macrophage culture

For *in vitro* differentiation of mouse bone marrow cells into bone marrow-derived macrophages (BMDMs), both tibias and femurs were flushed with up to 30 mL of DPBS (Ca^{2+} and Mg^{2+} free). Cell extracts were then washed and seeded into non-tissue-culture treated 6-well plates (cat.# 229506, CELLTREAT, MA, USA) (2E6 cells/well) or T-75 (cat.# CC7672-4875, USA Scientific, FL, USA) (50E6 cells), and cultured for 6—7 days in 3 mL or 10 mL, respectively, of DMEM/F12 (cat.# 10565018, Thermo Fisher) supplemented with 10% heat-inactivated FBS, 100 U/mL penicillin, 100 μg/mL streptomycin, 17.5 mM D-Glucose, 2.5 mM Glutamax, 0.5 mM sodium pyruvate (BMDM media), and 40 ng/mL mouse recombinant M-CSF (cat.# 78059, STEMCELL Technologies). Cells were replenished with fresh BMDM media on day 2, 4 and 6, and lifted on day 6 by incubating with pre-warmed accutase at 37 °C for 5 min followed by gentle scraping. Cell aliquots were subjected to either flow cytometric analysis or extracellular flux analysis. For the Seahorse extracellular flux analysis, 1E5 BMDM cells/well were seeded with 300 μL BMDM media in a Seahorse XF 96-well culture plate (tissue culture treated) and incubated overnight at 37 °C, 5% CO_2.

2.6. Lipid mediator quantification by targeted liquid chromatography-tandem mass spectrometry (LC-MS/MS)

To quantify differences in lipid mediators, mice were euthanized and 2—3 mL of cell-free peritoneal lavage fluid was isolated from sedentary and exercise mice and immediately frozen at −80 °C. On the day of extraction, samples were thawed on ice, volumes recorded, and incubated in two volumes of ice-cold methanol containing 500 pg of deuterium-labeled internal standards (i.e. Resolvin D2-d_5, Resolvin D3-d_5, Maresin 1-d_5, Maresin 2-d_5, Lipoxin A4-d_5, Resolvin E1-d_4, 5(S)-HETE-d_8, 15(S)-HETE-d_8, (+)11(12)-EET-d_{11}, 15-deoxy-Δ12,14-Prostaglandin J2-d_4, Prostaglandin E2-d_4, and Leukotriene B4-d_4) to determine extraction efficiency. Samples were then placed at −80 °C for 45 min to promote protein precipitation. Protein precipitates were pelleted by centrifuging samples at 6200 RCF for 10 min at 4 °C and supernatants were transferred into 12 mL borosilicate glass round-bottom tubes. Supernatants were dried to ∼400 μL in a Biotage TurvoVap Classic by the addition of a gentle stream of N_2 gas while keeping tubes at 37 °C. Samples were then acidified by the addition of pH 3.5 HPLC-grade H_2O and promptly loaded onto Biotage ISOLUTE C18 SPE columns (cat.# 220-0020-c, Biotage), which were pre-equilibrated with 3 mL of HPLC-grade MeOH and 3 mL HPLC-grade H_2O. After samples were loaded, columns were then neutralized with 5 mL of HPLC-grade H_2O and subsequently treated with 5 mL of HPLC-grade hexane to remove neutral lipids. Lipid mediators of interests were then eluted and collected by the addition of 5 mL HPLC-grade methyl formate. Samples were dried to completion with a gentle stream of N_2 gas in a 37 °C water bath and immediately resuspended in 50 μL of MeOH:H_2O (50:50 v/v). For LC-MS/MS analysis, samples were injected onto a Kinetex Polar C18 HPLC column (100 mm length x 3 mm diameter; 2.6 μm particle size; 100 Å pore size) (cat.# 00D-4759-Y0, Phenomenex, California, USA) maintained at 60.6 °C using a Shimadzu LC-20AD with a SIL-20AC autoinjector (Shimadzu, Kyoto, JP), coupled to a 5500 Qtrap (AB Sciex, Toronto, CA). Targeted LC-MS/MS analysis was carried first by gradient elution of lipid mediators with a constant 0.5 mL/min mobile phase delivery, initially consisting of 45:55:0.01 (v/v/v) methanol:water:acetic acid, which was then ramped up to 80:20:0.01 over 16.5 min, and then to 98:2:0.01 over the next 2 min. The 5500 Qtrap was operated in negative polarity mode. All data were acquired using Analyst v1.7.1 and analyzed with Sciex OS-Q v3.0.0.3339.

Each analyte was identified using multiple reaction monitoring (MRM) and enhanced product ion (EPI) mode (Supplemental Table S1) with retention time (RT) matching to synthetic standards (Fig. S1B). A given chromatographic peak was quantified if the following criteria were met: (1) RT was within +/− 0.1 min of the synthetic standard's RT; (2) chromatographic peak was composed of at least 5 points across

baseline; (3) MS/MS spectra at the appropriate RT contained at least 6 diagnostic ions; (4) signal-to-noise ratio (SNR) was greater than 3; (5) the calculated analyte concentration was greater than the empirically-determined LLOD and LLOQ for the respective analyte.

Determination of the lower limit of detection (LLOD) and lower limit of quantitation (LLOQ) was carried out as recommended by the International Council for Harmonization analytical guideline Q2 (R2) (https://www.ich.org/page/quality-guidelines). Briefly, for all analytes, calibration standards (Cayman Chemical) were prepared by mixing twelve synthetic standards with a beginning concentration of 100 pg/μl (Standard 1) and serially diluted in HPLC-grade methanol (Sigma–Aldrich) by 1:2 to a final concentration of 0.048 pg/μl (Standard 12). For each standard, an injection volume of 5 μl was used. At least five independent injections of each standard were used to generate data to determine LLOD and LLOQ for each analyte. From the accumulated data, the slope (S) of the calibration curve and the standard deviation (σ) of the y-intercept, which represents the blank condition, were calculated. LLOD and LLOQ were calculated using $3.3*\sigma/S$ and $10*\sigma/S$, respectively.

Lipidomics data was analyzed using MetaboAnalyst 5.0 (metaboanalyst.ca). Analytes missing data in more than 50% of the samples were removed and missing values were imputed with 1/5 of the minimum positive value. Data were log transformed and autoscaled before analysis, as described in Fredman et al. [24]. Global changes between groups were compared using Student's *t*-tests ($P < 0.05$) and a fold-change threshold of 1.5.

2.7. Real-time extracellular flux (XF) analysis

After 3h (PM) or overnight incubation (hMDM and BMDM), cells were washed twice with 200 μL Seahorse XF DMEM medium per well (free of sodium bicarbonate, phenol red, and serum, pH 7.4; cat.# 103575-100, Agilent Technologies). For PM and BMDM cells, XF DMEM was supplemented with 24 mM D-Glucose, 4 mM L-Glutamine and 1 mM sodium pyruvate; for hMDM, the medium was supplemented with 11.1 mM D-Glucose, 2 mM L-Glutamine and 1 mM sodium pyruvate. These supplemented media formulations will henceforth be referred to as XF media. Cells were either left untreated or treated with the respective SPM compounds at the indicated concentrations for 2 h, while incubating at 37 °C and at normal atmospheric CO_2 partial pressure. The lack of added CO_2 to incubator air for 1–2 h is a manufacturer-recommended step to facilitate removal of dissolved CO_2 gas from culture media and all culture vessel materials, which is crucial for proper OCR and ECAR measurements on the Seahorse XF analyzer. Where indicated, BMDM were washed with XF DMEM after overnight culture, and incubated with 500 nM Compound C (CompC) for 30 min before 2 h incubation with 1 nM of the indicated SPM (e.g., RvD1, RvD2, RvE1, MaR1).

After 2 h incubation, cells were subjected to either continuous readings for 80 min or to a mitochondrial stress assay where indicated in the Seahorse XFe96. For this assay, oligomycin, FCCP, and Antimycin-A/Rotenone (cat. # O4876-5 MG, C2920-10 MG, A8674-50 MG and R8875-1G, respectively, MilliporeSigma) solutions were successively added (without washing away the previous compound) to each well at the indicated time points. Assay configuration: 80-min total; 6-min interval between each datapoint, with 3 min spent mixing and 3 min reading, for each datapoint. The following working concentrations of mitochondrial inhibitors were used for the respective cell type, as determined by dose response titrations performed beforehand in separate experiments (data not shown): For PM and BMDM: 1.5 μg/mL oligomycin, 1.5 uM FCCP, 10 uM Antimycin-A, 1 uM Rotenone. For hMDM: 2 μg/mL oligomycin, 2 uM FCCP, 10 uM Antimycin-A, 2.5 uM Rotenone.

The following formulas were used to calculate the indicated mitochondrial respiratory parameters: Non-Mitochondrial OCR = minimum OCR value achieved after Antimycin-A + Rotenone (AA/R) injection; Basal OCR = (last OCR value before oligomycin injection) − (Non-Mitochondrial OCR); Maximal OCR = (max OCR value after FCCP injection) − (Non-Mitochondrial OCR); ATP-Linked OCR = (last OCR value before oligomycin injection) − (minimum OCR value achieved after oligomycin injection); Spare Respiratory Capacity = (Max OCR) − (Basal OCR); Spare Respiratory Capacity as % of Basal = [(Max OCR)/(Basal OCR)] x 100%; H^+ Leak = (minimum OCR value after oligomycin injection) − (Non-Mitochondrial OCR); % Coupling Efficiency = [(ATP-Linked OCR)/(Basal OCR)] x 100%.

2.8. Flow cytometric analysis

For all experiments except TMRM staining and intracellular pAMPK staining, ice cold FACS buffer (DPBS, Ca^{2+}/Mg^{2+} free, with 1% FBS) was used for washing, FcR blocking, staining, and running samples. All incubations were done in the dark with tubes on ice. For TMRM staining of BMDM cells, pre-warmed, XF media (see recipe above; additionally supplemented with 10 mM EDTA and 10% FBS) was used for washing, FcR blocking, staining, and running samples, and samples were kept at 37 °C at all times.

1E5 (BMDM and hMDM) or 1E6 (PM) cells were aliquoted, per sample, after either peritoneal lavage (PM) or accutase digestion (BMDM and MDM). Cells were washed once and resuspended and incubated for 10 min on ice or at 37 °C (for TMRM experiments) in 50 μL of an Fc receptor blocking solution (for mouse BMDM and PM: 0.5 μg of a rat anti-mouse CD16/CD32 monoclonal Ab, clone 93 [cat.# 14-0161-82, Thermo Fisher]; for hMDM: 5 μL of Human BD Fc Block, clone Fc1.3216 [cat.# 564220, BD] Biosciences). After FcR blocking, 50 μL of a staining solution was added for a total staining volume of 100 μL. The following primary flow cytometry Ab (See Table S2 in Supplemental Methods) were incubated together at the indicated amounts in a 100 μL staining volume:

For PM: CD45-FITC, F4/80-PE, CD64-BV421 and Ly6G-APC. For BMDM: CD45-FITC and CD64-BV421 were used as indicated above, with F4/80-eFluor 660 added to the flow cytometric panel. For hMDM, the following Ab were used: CD14-StarBright Violet 610, CD16-FITC, CD206-APC and CD64-BV421.

For TMRM staining of BMDM or PM: 40 nM TMRM (cat.# I34361, Thermo Fisher) was added with other primary flow cytometry antibodies (CD45-FITC, F4/80-eFluor 660 and CD64-BV421) and was incubated for 30 min at 37 °C in the dark. For all other flow cytometry experiments not involving TMRM staining, samples were stained for 30 min, on ice, in the dark. After staining, samples were washed with 5X volumes of either ice-cold flow buffer or 5 × volumes of pre-warmed XF media (for TMRM experiments on BMDM or PM) before centrifuging and resuspending samples in the respective solution before submitting samples for flow cytometric analysis.

All data were analyzed using BD FlowJo v10.8.1. To generate a t-SNE map of PM stained with cell surface markers CD45-FITC, F4/80-eFluor660, CD64-BV421 and lipophilic potentiometric dye, TMRM, all FCS files were cleaned up by removing doublets and cell debris. A subset of 10,000 events per sample were randomly chosen using DownSampleV3 FlowJo plug in and concatenated into a single FCS file containing all events to create a dataspace representative of all possible cell populations. The sample identity for each event from each individual FCS file was maintained by creating a Sample ID parameter

during the concatenation process. The t-SNE map was created using the concatenated file, using the opt-SNE algorithm implementation developed by Belkina et al. [30] with the following hyperparameters: Iteration number = 1000, Perplexity = 30, learning rate (eta) = 15783), KNN algorithm: Exact (vantage point tree), gradient algorithm: Barnes-Hut. The FlowSOM algorithm developed by Van Gassen et al. [31] was ran on the same concatenated file using the following hyperparameters: number of metaclusters = 12, SOM grid size (W x H) = 10 x 10. The TMRM MFIs for the respective FlowSOM populations were then extracted for each individual sample using a sample ID parameter created during the FCS file concatenation process, as described above.

2.9. Intracellular detection of p-AMPKα1(Thr172) by flow cytometry

1E6 PMs from C57BL/6J WT mice were incubated with 20 μM Compound C (stock: 2.5 mM in DMSO) or Veh for 2h at 37C in incubation media (RPMI1640, 10% FBS, 1X GlutaMAX) before being washed and incubated with 100 μM metformin (stock: 100 mM in water; cat # 317240, Millipore Sigma), in the presence of CompC or Veh, for 30 min at 37C. Cells were then washed with Ca^{2+}/Mg^{2+} free DPBS, spun down and resuspended in 750 μL of Cytofix/Cytoperm solution (cat.# 554714, BD Biosciences) per sample, and incubated for 20 min on ice. After fixing and permeabilizing, cells were washed twice with 3 mL of 1X Perm/Wash buffer (cat.# 554714, BD Biosciences), and then spun down and resuspended in 50 μL of an FcR block solution in Perm/Wash buffer (0.5 μg of a rat anti-mouse CD16/CD32 monoclonal Ab, clone 93 [cat.# 14-0161-82, Thermo Fisher]) and incubated for 10 min on ice. Cells were then stained with a polyclonal, rabbit anti-mouse FITC-labeled p-AMPKα1(Thr172) antibody (Biorbyt, cat. # orb8540) in a 100 μL staining volume (perm/wash buffer) and incubated 30 min on ice. Tubes were washed twice with 3 mL of perm/wash buffer and finally centrifuged and resuspended in FACS buffer before analyzing samples. All data was acquired on a BD LSR-Fortessa X-20 flow cytometer equipped with 4 lasers (Violet 405 nM, Blue 488 nM, Yellow-green 561 nM, and Red 640 nM) and using FACSDiva v8.03.

2.10. Confocal laser scanning microscopy (CLSM)

BMDM were cultured as previously described. Cells were harvested at the end of day 6, as described above, and 1.75E6 cells were re-seeded in 35 mm glass bottom dishes (14 mm glass diameter) (cat.# P350G-0-14-C, MerTek) in 3 mL of BMDM media. After overnight incubation and without washing away culture media, 5 nM TMRM (cat. # I34361, Thermo Fisher) and 5 μg/mL Hoechst 33342 (cat. # H3570, Thermo Fisher) were directly added to the cells and allowed to incubate for 30 min at 37 °C, in the dark. After incubation, 3 mL of staining solution was carefully removed as to not disturb cells, 2 mL of pre-warmed XF media was added, and imaged for Hoechst and TMRM. Immediately after capturing images, FCCP was directly added to the dish at a final concentration of 25 uM, incubated in the dark at room temperature for 10 min, and re-imaged. Images were taken on a Nikon A1 CLSM, mounted on a Nikon TE-2000E2 microscope body, using a Plan Apo 60X/NA 1.4 Oil objective. Images were produced with a Galvano scanner at $^1/_2$ frame per second (1024 × 1024 pixels), one-way scanning with line averaging value of 2, a scanner zoom value of 1, and pinhole size of 39.7 μm. Hoechst 33342 fluorescence emission was captured using a 405 nm solid state laser at 2% power, using a 450/50 long pass (LP) filter, and setting PMT voltage gain at 100. TMRM fluorescence emission was captured using a 561 nm solid state laser at 2.5% power, using a 525/50 LP filter, and setting PMT voltage gain at 100. The transmitted light channel (TL-DIC) was captured via transmitted light DIC technique, setting the transmitted light PMT detector gain at 120.

2.11. Immunoblotting analysis

Bone marrow cells/well were seeded (non-tissue culture treated 6-well plate) in 3 mL BMDM media and cultured for 6 days as described above. On day 6, media was removed, and 3 mL fresh BMDM media containing 1 nM RvD1 or not was added for 1h before removing media and collecting cell lysate in 100 μL of ice-cold lysis buffer per well. Lysis buffer was composed of 50 mM HEPES, 5 mM EDTA, 150 mM NaCl, 1% (v/v) NP-40, 0.1% (w/v) SDS, 1X Halt Protease inhibitor cocktail (cat.# 87785, Thermo Fisher) and 1X Halt Phosphatase inhibitor cocktail (cat.# 78420, Thermo Fisher). Protein concentration was determined using Pierce BCA protein assay kit (cat.# 23227, Thermo Fisher). 60 μg of protein per sample was mixed with 1X Laemmli sample buffer (cat.# 1610747, BioRad) and resolved on a 10% Criterion TGX Precast Midi SDS-PAGE gel (cat.# 5671033, Bio-Rad) and electrotransferred to Immun-Blot PVDF membranes (150–160 μg/cm^2) (cat.# 1620177, BioRad). Membranes were blocked with 5% (w/v) non-fat milk (cat.# M–0841, LabScientific, MA, USA) in TBST buffer (TBS containing 0.1% Tween-20) for 1h. The membrane was then probed overnight with rabbit phospho-AMPKα (Thr172) (1:1000; cat.# 2535S, Cell Signaling Technology, MA, USA) antibody diluted in 5% (w/v) BSA in TBS-T. The blot was washed three times in TBST and incubated with anti-rabbit HRP-conjugated secondary IgG (1:2000; cat.# 7074S, Cell Signaling Technology) in 5% (w/v) non-fat milk for 1h. The membrane was washed 3 times in TBST and then incubated with Pierce ECL Plus (cat.# 32132, Thermo Fisher) and imaged using an MYECL Western Blotting Detection System (Thermo Fisher). After imaging, the membrane was stripped using Restore Western Blot Stripping Buffer (cat.# 21059, Thermo Scientific) and re-probed with mouse AMPKα (1:1000; cat.# 2793S, Cell Signaling Technology) to normalize p-AMPKα expression.

2.12. RT-qPCR

Human MCSF-MDM and GMCSF-MDM were harvested after 6 days of differentiation culture and whole-cell RNA was isolated and purified using RNeasy Mini Kit (cat. # 74106, Qiagen; Hilden, Germany), performing DNA digestion with RNase-free DNase I Set (cat#. 79256, Qiagen) before eluting. RNA concentration and purity were determined by UV absorbance spectrophotometry with a NanoDrop 2000c (Thermo Fisher). cDNA was prepared by reverse transcription PCR using 1 μg of RNA as template and using MultiScribe Reverse Transcriptase with the random primers scheme for initiation of cDNA synthesis (part of the High Capacity cDNA RT Kit; cat.# 43-688-13, Thermo Fisher). PowerUP SYBR Green Master Mix (cat.# A25776, Thermo Fisher) with Dual-Lock Taq DNA polymerase and ROX as passive reference dye was used for quantitative RT-PCR in an Applied Biosystems QuantStudio 5 (Thermo Fisher). All manufacturer's recommended steps were followed. Validated, commercially available PCR primers (see primer information in Table S3 of Supplemental Methods) were purchased from Qiagen (RT^2 qPCR Primers, cat#. 330001) and used for quantitative PCR assays. The $2^{-\Delta\Delta CT}$ method was used to calculate relative expression following normalization to the housekeeping gene *Hprt*.

2.13. Study approval

All murine procedures were performed under approved protocols by the University of Louisville Institutional Animal Care and Use Committee (#20732) and institutional biosafety committee (#21–295). Mixed human venous peripheral blood was collected under an approved

protocol from the University of Louisville's Institutional Review Board (21.0688) from de-identified donors following written consent.

2.14. Statistical analysis

Results are expressed mean ± standard error of the mean (SEM) of n observations, where n represents the number of biological replicates per experimental group. All animals were randomly assigned to experimental groups and age matched with proper controls. All statistical comparisons were performed with GraphPad Prism v9.3.1. Statistical comparisons between two groups were conducted using either paired or unpaired two-tailed Student's *t* test, while comparisons of multiple groups were performed using one-way ANOVA or two-way ANOVA, where appropriate, with Holm-Šídák's post hoc tests. In all cases, statistical significance was set at $P < 0.05$. Sample sizes and *p* values (for the indicated pair-wise comparisons) for the respective graphs are indicated in figure legends.

3. RESULTS

3.1. Exercise induces SPM biosynthesis and enhances mitochondrial respiration in macrophages

Consistent with published literature [32], voluntary wheel running provided a robust model of aerobic exercise training in C57BL6 mice, as evidenced by high levels of wheel running activity (~4 km per day at ~ 0.25 m/s average speed) (Fig. S1A). To examine whether exercise training affects lipid mediator production and cellular metabolism of macrophages, peritoneal exudates collected from sedentary and exercise-trained mice were subjected to targeted LC-MS/MS lipidomic analysis, while intraperitoneal leukocytes, of which ~85% are elicited peritoneal macrophages (PM), were subjected to extracellular flux (XF) analysis, respectively (Figure 1A). Using a data dimensionality reduction approach, we found that Partial Least-Squares Discriminate Analysis (PLS-DA) of lipid mediator concentrations resulted in distinct group clustering of sedentary and exercise animals (Fig. 1B). A summary of fold change analysis of individual lipid mediators is presented as a heat map (Fig. 1D). Exercise increased the concentration of the proresolving lipid mediator RvE1, while also increasing the levels of 20-OH-LTB_4, PGJ_2, and 13,14-dihydro-15-keto-PGE_2; breakdown metabolites of pro-inflammatory lipid mediators LTB_4, PGD_2, and PGE_2, respectively (Fig. 1C). Likewise, exercise induced a decrease in the arachidonic acid metabolite, 5*S*,15*S*-diHETE, which has been shown to be an eosinophil chemoattractant and neutrophil degranulation agonist [33–35] (Fig. 1C). These data suggested that exercise promotes the production of proresolving lipid mediators and metabolic breakdown of pro-inflammatory lipid mediators. In support of this, we found that the ratio of 5-lipoxygenase (5-LO) derived proresolving (e.g., RvE1 and RvD1) to pro-inflammatory (e.g., LTB_4, 6-*trans* LTB_4, and 6-*trans*-12-*epi* LTB_4) lipid mediators is increased following exercise.

We next asked whether the observed exercise-induced upregulation of RvE1 biosynthesis was associated with changes in PM intermediary metabolism. To this end, we found that four weeks of wheel running resulted in enhanced basal, ATP-linked, maximal, and spare mitochondrial respiratory capacity (Figure 1E–F) in PM, indicating that exercise promotes SPM production and mitochondrial metabolism in macrophages.

3.2. SPMs stimulate mitochondrial metabolism in macrophages

Given that exercise increased proresolving lipid mediator RvE1 levels and mitochondrial respiration, we asked whether RvE1 and other SPMs directly alter mitochondrial metabolism in PMs isolated from control mice (Figure 2A). We found that 1 h incubation with 1 nM RvD1, RvD2, RvE1 and MaR1 stimulated basal and ATP-linked respiration with a mean increase in maximal respiration in PMs (Figure 2B–C). Moreover, the observed increase in basal respiration at the start of the mitochondrial stress assay persisted for over 60 min (Figs. S2A–S2E), suggesting that SPM signaling pathways contribute to sustained increases in mitochondrial respiration in macrophages.

3.3. RvD1 and RvE1 differentially alter mitochondrial metabolism in human macrophages

Given that exogenous RvE1 and RvD1 treatment enhanced mitochondrial metabolism in murine PM, we explored whether these effects were also common to human monocyte-derived macrophages (MDM) differentiated in the presence of either M-CSF (MCSF-MDM) or GM-CSF (GMCSF-MDM). We first characterized MDM cell surface expression of monocyte-macrophage lineage markers following hematopoietic growth factor treatment, MCSF-MDM and GMCSF-MDM (Figure 3A–B). As previously reported [36–39], the hematopoietic growth factors for *in vitro* differentiation of MCSF-MDM and GMCSF-MDM did not differentially alter expression of canonical M1 (CD64) or M2 (CD206) (Figure 3A–B) cell surface markers. However, as reported previously [40], CD14 and CD16 were differentially expressed: CD14 expression was approximately 7-fold higher in MCSF-MDM compared to GMCSF-MDM, while CD16 expression was approximately 2.6-fold higher in MCSF-MDM relative to GMCSF-MDM (Fig 3B). These findings were associated with increased cellular respiration and extracellular acidification rates in GMCSF-MDM compared to MCSF-MDM. Results of which are consistent with human GM–CSF–derived macrophages having higher oxidative phosphorylation activity [41].

As expected, SPM-mediated enhancements in cellular metabolism observed in murine PM was also observed in human GMCSF-MDM, whereby 1h incubation with 1 nM RvD1 increased basal and ATP-linked mitochondrial respiration (Figure 3C–D). Surprisingly, stimulation of mitochondrial respiration was not recapitulated in MCSF-MDM cells (Figure 3E–F). RvD1 treatment, and not RvE1, resulted in stimulating mitochondrial respiration only in GMCSF-MDM, which may have resulted from down regulation of the RvE1 receptor CHEMR23 following GMCSF-MDM differentiation (Fig. S3). Nevertheless, these data suggest that proresolving signaling pathways also promote mitochondrial metabolism in human GMCSF monocyte-derived macrophages.

3.4. RvD1 stimulated macrophage mitochondrial metabolism is dependent on FPR2 signaling

To assess whether RvD1-enhanced mitochondrial respiration in macrophages is receptor-mediated, we subjected murine PM isolated from $Fpr2^{+/+}$ and $Fpr2^{-/-}$ mice to 0.1 nM, 1 nM and 10 nM RvD1. Notably, PM lacking FPR2 receptor expression display no change in mitochondrial respiration following RvD1 treatment (Figure 4A, C). This was indicated by no significant differences in basal, ATP-linked, or maximal mitochondrial respiration (Figure 4B, D). Additionally, lack of stimulation of basal respiration in $Fpr2^{-/-}$ PM was persistant, while, as previously observed (Fig. S2), $Fpr2^{+/+}$ PM had a sustained increase in basal respiration following RvD1 treatment (Fig. S4).

Given that basal respiration was elevated in $Fpr2^{-/-}$ PM relative to $Fpr2^{+/+}$ PM (Fig. 4F), we immunophenotyped PM via flow cytometry to assess potential differences in recruited population abundances that may account for the observed difference. As shown in Figure 4G–H, the lack of FPR2 expression did not alter the abundance of total $CD45^+$ cells, $CD45^+Ly6G^+$ neutrophils, small ($CD45^+F4/80^{low}$) PM, or large ($CD45^+F4/80^{high}$) PM (Figure 4G–H). From these data, we infer that

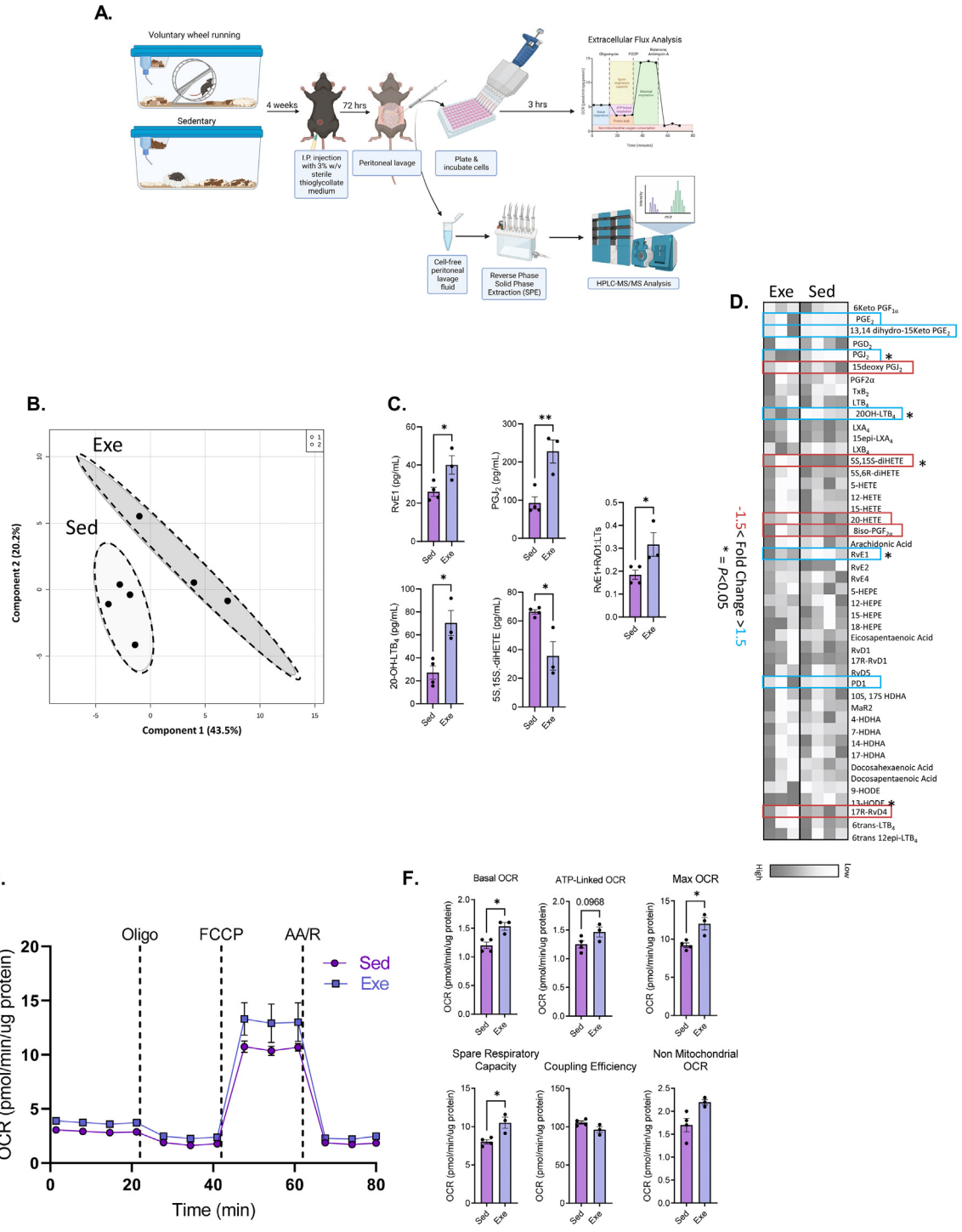

Figure 1: Exercise induces SPM biosynthesis and mitochondrial respiration in macrophages. (**A**) Experimental scheme outlining the isolation of PM from exercise-trained mice and subsequent assessment of mitochondrial respiratory parameters via extracellular flux (XF) analysis, as well as extraction and quantification of lipid mediators in the cell-free lavage fluid via SPE and HPLC-MS/MS, respectively. (**B**) Partial Least Squares-Discriminant Analysis (PLS-DA) and (**D**) heatmap of peritoneal lipid mediator metabololipidomics following four weeks of voluntary wheel running (Exe) or sedentarism (Sed). (**C**) Quantification of RvE1, PGJ_2, 20-OH LTB_4, 5*S*,15*S*-diHETE and ratio of RvE1 and RvD1 to leukotrienes (LTs; LTB_4, 6-*trans* LTB_4, and 6-*trans*-12-*epi* LTB_4). (**E**) Cellular respiration was assessed by recording oxygen consumption rate (OCR) of peritoneal macrophages (PM) isolated from exercise and sedentary mice. (**F**) Derived mitochondrial respiratory parameters calculated from the mitochondrial stress assay. Data expressed as mean ± SEM, $n = 4$ for Sed mice, $n = 3$ for Exe mice. $^{*}P < 0.05$, $^{**}P < 0.01$, two-tailed Student's *t*-test.

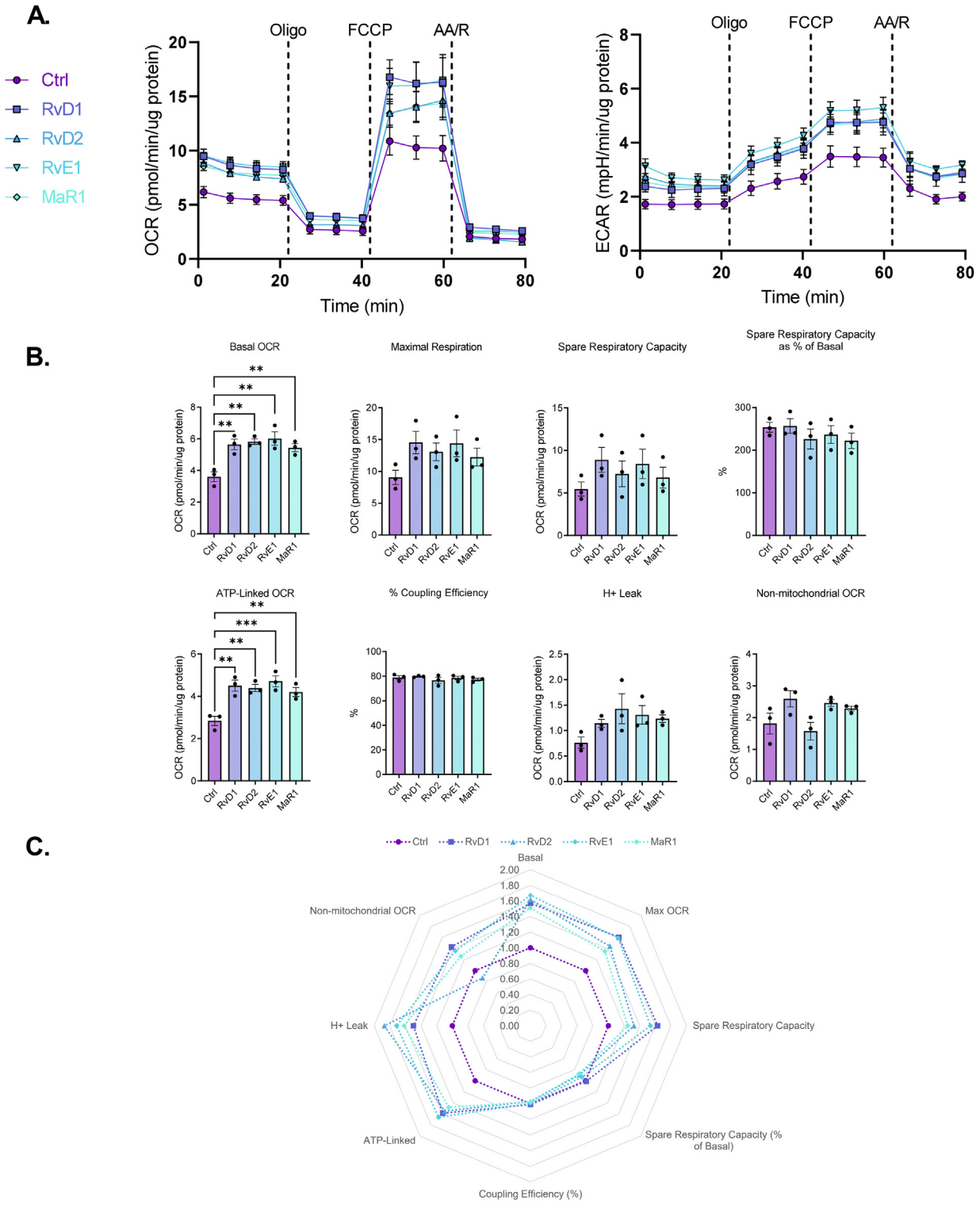

Figure 2: SPMs stimulate mitochondrial metabolism in peritoneal macrophages. (**A**) PM from non-exercised mice were treated without or with 1 nM of the indicated SPM (RvD1, RvD2, RvE1, or MaR1) for 1h prior and throughout OCR and ECAR measurements of a mitochondrial stress assay. (**B**) Derived mitochondrial respiratory parameters were quantified and (**C**) fold changes of each respiratory parameter for each SPM treatment vs control are summarized in radar plots. Data expressed as mean ± SEM, $n = 3$ for all groups; $^{**}P < 0.01$, $^{***}P < 0.001$; One-way ANOVA with Holm-Šídák post-test.

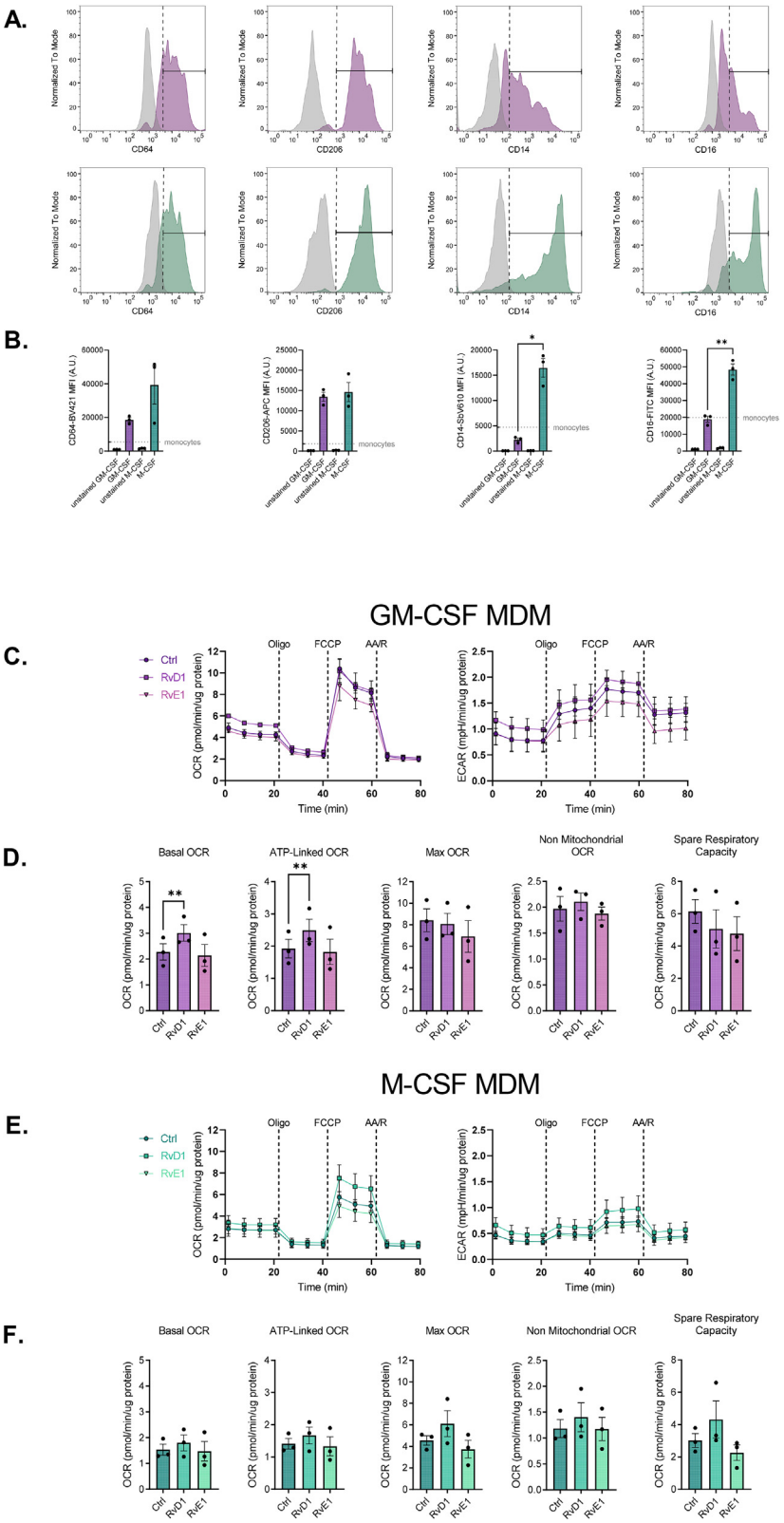

Figure 3: RvD1, but not RvE1, stimulates mitochondrial metabolism in human macrophages. (**A**) Human PBMC were subjected to flow cytometric analysis to quantify expression level of monocyte-macrophage cell surface markers. Unstained samples shown in grey histograms while stained ones are shown in respective colored histograms: GM−CSF−differentiated hMDM in purple (top row) while M−CSF−differentiated hMDM are shown in green (bottom row). (**B**) Quantification of CD14, CD16, CD64, and CD206 MFI following differentiation in GM-CSF and M-CSF. Grey dashed line shows the MFI for the respective marker on undifferentiated hPBMC. (**C**, **E**) Oxygen consumption rate (OCR) and extracellular acidification rate (ECAR) values following treatment without or with 1 nM RvD1 or RvE1 in GM-CSF or M-CSF differentiated MDM. (**D**, **F**) Quantification of derived mitochondrial respiratory parameters. Data expressed as mean ± SEM; $n = 3$ for all groups; $^{**}P < 0.01$; One-way ANOVA with Holm-Šídák post-test.

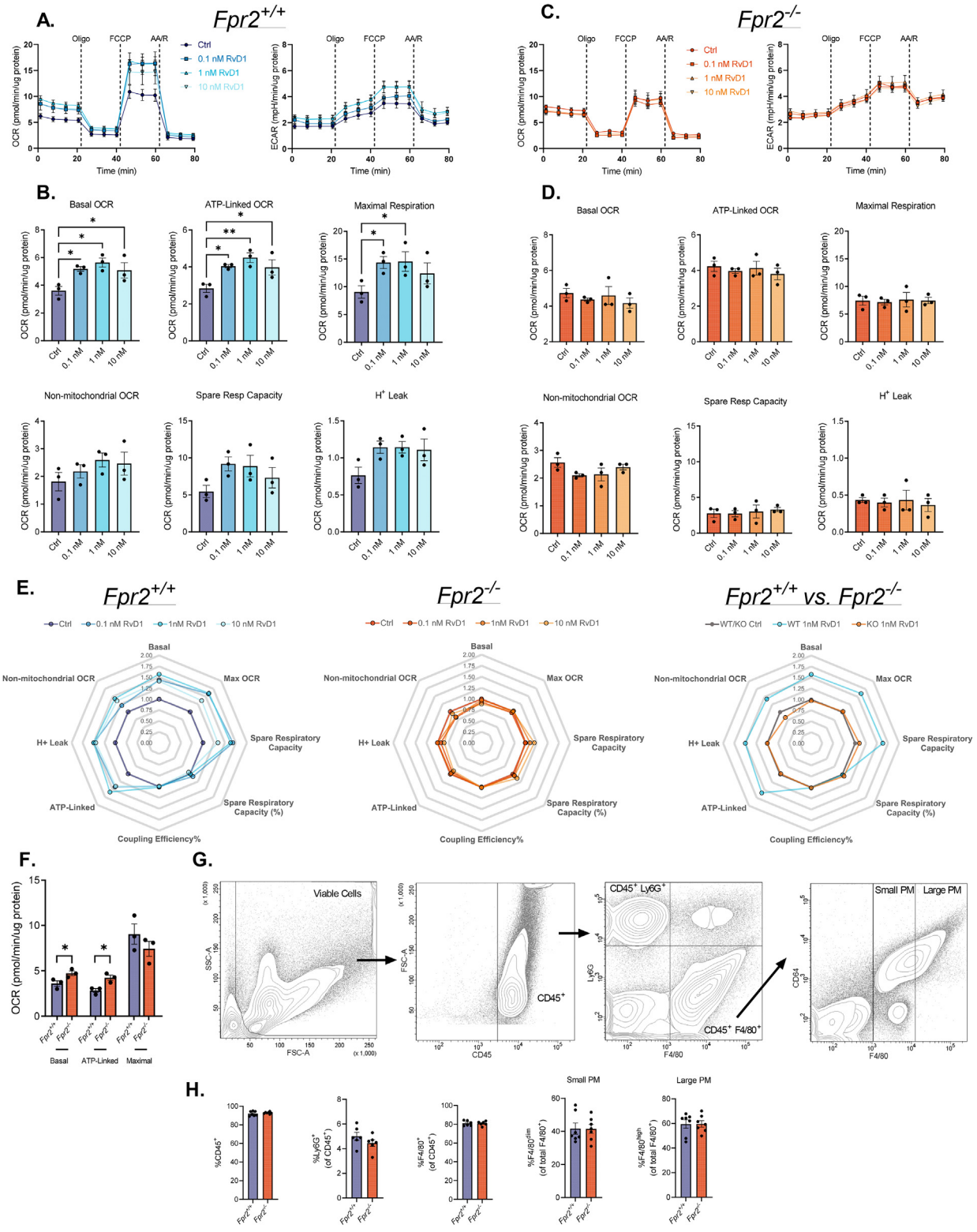

Figure 4: RvD1 stimulated mitochondrial metabolism in macrophages is dependent on FPR2 signaling. (**A**, **B**, **E**) PM from non-exercised *Fpr2*$^{+/+}$ or (**C**, **D**, **E**) *Fpr2*$^{-/-}$ mice were treated without or with 0.1 nM, 1 nM, or 10 nM RvD1 for 1h prior to, and throughout, (**A**, **C**) OCR and ECAR measurements of a mitochondrial stress assay. (**B**, **D**) Derived mitochondrial respiratory parameters were quantified for macrophages isolated from (**B**) *Fpr2*$^{+/+}$ and (**D**) *Fpr2*$^{-/-}$ mice, and (**E**) fold changes of respiratory parameters for each SPM treatment vs. control are summarized in radar plots. (**F**) Basal, ATP-linked and Maximal OCR for PM isolated from *Fpr2*$^{+/+}$ and *Fpr2*$^{-/-}$ mice. (**G-H**) PM aliquots were subjected to immunophenotyping via polychromatic flow cytometric analysis to assess expression levels of cell surface markers diagnostic of mature, large (CD45^{+}F4/80^{high}) and small (CD45^{+}F4/80^{low}) peritoneal macrophages, as well as neutrophiles (CD45^{+} Ly6G^{+}). (**H**) Percent of CD45^{+} cells quantified out of viable, doublet-excluded cells. %Ly6G^{+} and %F4/80^{+} cells quantified out of viable, doublet-excluded, CD45^{+} cells. %F4/80^{dim} and %F4/80^{high} cells quantified out of viable, doublet excluded, CD45^{+} F4/80^{+} cells. Data expressed as mean ± SEM; $n = 3$ in (**A-F**) and for $n = 6–7$ in (**G-H**); $^{*}P < 0.05$, $^{**}P < 0.01$; One-way ANOVA with Holm-Šídák post-test (**B**, **D**) or two-tailed Student's *t*-test (**F**—**H**).

deletion of FPR2 results in compensatory mechanisms that increase basal and ATP-linked respiration. Nonetheless, these data collectively suggest that RvD1-induced stimulation of mitochondrial respiration in macrophages is mediated via FPR2 signaling.

3.5. SPMs stimulate mitochondrial metabolism in BMDMs

To assess whether SPM-mediated stimulation of mitochondrial respiration extends beyond peritoneal macrophages, we examined the effect of SPM signaling on mitochondrial function in bone marrow-derived macrophages (BMDMs). BMDMs were treated with 1 nM RvD1, RvD2, RvE1 or MaR1 and subjected to a mitochondrial stress assay (Figure 5A—B). Similar to murine PM and human MDM, murine BMDMs treated with RvD1, RvD2, RvE1 and MaR1 display enhanced basal and ATP-linked mitochondrial respiration, while maximal respiration was significantly enhanced only by 1 nM RvD1 (Figure 5A—B). SPM-induced basal and ATP-linked mitochondrial metabolism in BMDMs was associated with changes in metabolic pathways (Figs. S5A—S5C). Similar to the stimulatory effect of SPMs in PMs, mitochondrial respiration in BMDMs was sustained following RvD1 incubation (Figs. S2F—S2G). These data are consistent with our PM results and suggest that RvD1 treatment increases $\Delta\Psi m$ and oxidative phosphorylation.

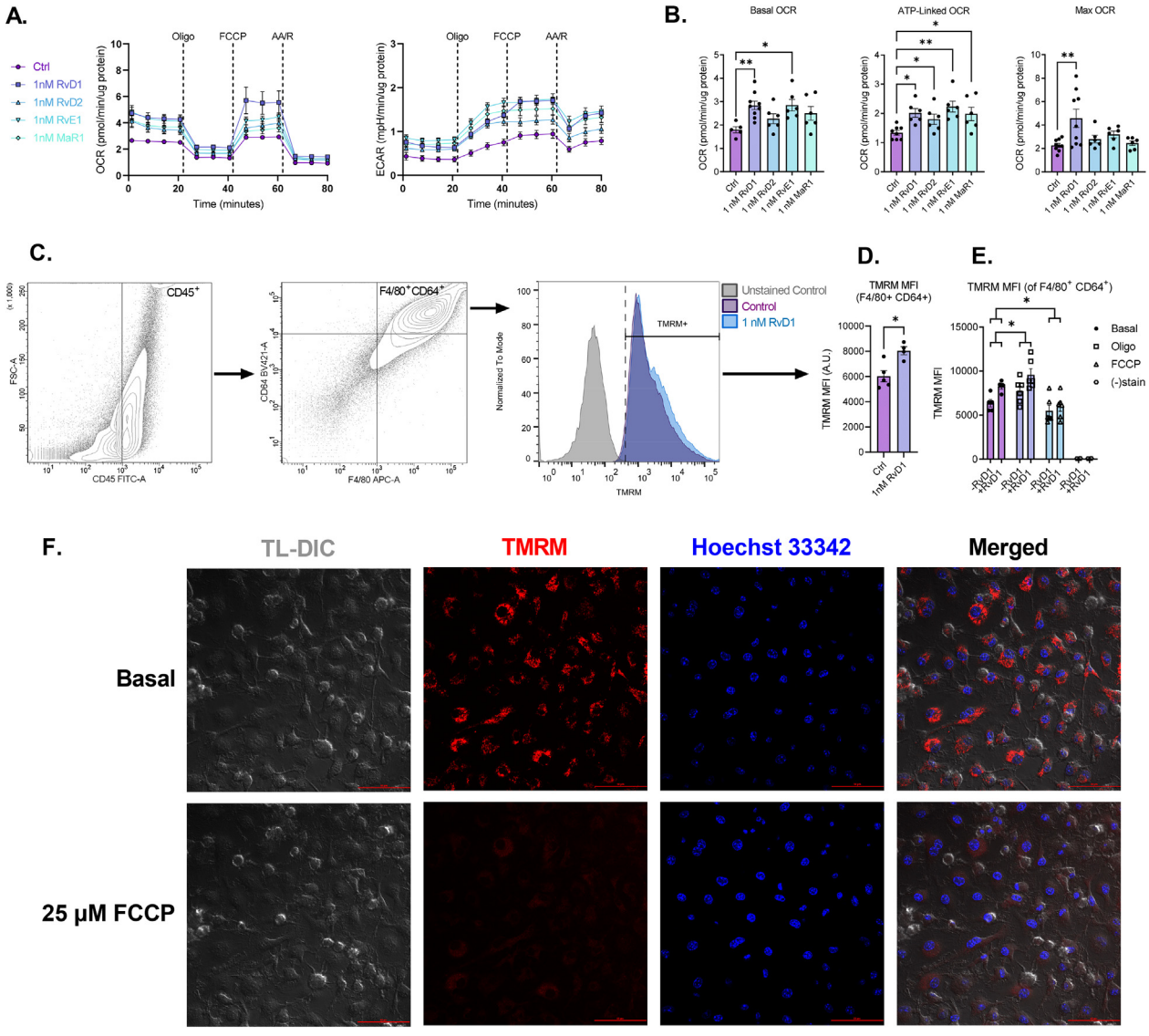

Figure 5: SPMs stimulate mitochondrial metabolism in BMDMs. BMDMs treated without or with indicated SPM and subjected to mitochondrial stress assay (**A-B**), flow cytometric analysis (**C-E**), or CLSM imaging (**F**). For the mitochondrial stress assay (**A-B**), BMDMs were treated without or with 1 nM of the indicated SPM (RvD1, RvD2, RvE1, or MaR1) for 1h prior to, and throughout 80 min of OCR and ECAR measurements (**A**) during a mitochondrial stress assay, for which the derived mitochondrial respiratory parameters are shown (**B**). For flow cytometric analysis (**C-E**), BMDMs were treated without or with 1 nM RvD1 and mitochondrial membrane potential, $\Delta\Psi m$, was quantified via TMRM mean fluorescence intensity (MFI), on $CD45^+$ $F4/80^+$ $CD64^+$ BMDMs (**D**). An aliquot of cells from the indicated groups was also treated with mitochondrial ETC complex inhibitors oligomycin and FCCP and resulting MFI recorded (**E**). BMDM from non-exercised mice were stained with Hoechst 33342 and TMRM, and imaged in the indicated fluorescent channels, or using TL-DIC technique on a confocal laser scanning microscope (**F**). Top row micrographs show cells in basal state (pre-FCCP incubation). Bottom row micrographs show cells after a 10-min FCCP incubation. Data expressed as mean ± SEM; $n = 3$—9 for all groups; $^*P < 0.05$, $^{**}P < 0.01$; One-way ANOVA with Holm-Šídák post-test (**B**), two-tailed Student's *t*-test (**D**), or two-way ANOVA with Holm-Šídák post-test (**E**).

Since the magnitude of the mitochondrial electrochemical proton motive force and respiratory chain activity (cellular OCR) are normally coupled, we evaluated changes in TMRM fluorescence intensity as an indication of mitochondrial function [42,43]. TMRM is a potentiometric, lipophilic, membrane permeable dye whose fluorescence intensity, under non-quenching conditions, correlates with mitochondrial membrane potential ($\Delta\Psi m$), (i.e., increased fluorescence equals increased polarized membrane potential). BMDMs, ~96% $CD45^+F4/80^+CD64$ (data not shown), were treated without or with 1 nM RvD1 for 1 h followed by the assessment of TMRM fluorescence. Following differentiation, 98% of BMDMs showed positive TMRM fluorescence values, indicating high BMDM vitality/viability (Figure 5C–D). Interestingly, TMRM mean fluorescence intensity (MFI) increased after 1 h treatment with 1 nM RvD1, indicating increased hyperpolarized mitochondrial membrane potential (Figure 5D–E). To assess the dynamic range of mitochondrial function, we treated BMDMS with the uncoupling protonophore FCCP, which resulted in a marked 13.6% and 27.7% decrease in TMRM MFI for control and RvD1-treated cells, respectively (Fig. 5E) [44–47]. To assess maximum $\Delta\Psi m$, we next added oligomycin, an ATP-synthase inhibitor that blocks H^+ re-entry into the mitochondrial matrix and thus drives a $\Delta\Psi m$ hyperpolarization [44]. As expected, TMRM MFI significantly increased above basal values (Fig. 5E).

To qualitatively assess TMRM staining and $\Delta\Psi m$, we utilized CLSM and observed, as expected, a significant reduction in TMRM fluorescence intensity following the addition of FCCP (Fig. 5F).

3.6. SPMs stimulate mitochondrial metabolism in macrophages through AMPK activation

Because AMPK plays a crucial role as master regulator of cellular bioenergetics and has been recently invoked in SPM signaling in macrophages [25,48–50], we posited that SPMs enhance mitochondrial respiration via AMPK-dependent signaling pathways. To test this, murine BMDMs were treated with either 1 nM RvD1, RvD2, RvE1 or MaR1 and expression of AMPK phosphorylation (Thr172) was measured by immunoblotting. RvD1 treatment resulted in a 40% increase in AMPK phosphorylation (Figure 6A). This prompted us to evaluate the AMPK dependence in SPM-stimulated mitochondrial respiration. For this, BMDMs were treated without or with Compound-C (CompC), an ATP-competitive inhibitor of AMPK kinase activity, and 1 nM RvD1 (Fig. 6B), RvD2 (Fig. 6C), RvE1 (Fig. 6D) or MaR1 (Fig. 6E). As observed before, 1 nM RvD1, RvD2, RvE1, and MaR1 increased basal and ATP-linked respiration. Treatment with CompC however prevented RvD1-, RvE1-, and MaR1-induced basal and ATP-linked respiration, but not RvD2 (Figure 6B–E), consistent with our immunoblotting data (Fig. S6A). These data suggest that RvD1, RvE1, and MaR1 stimulate mitochondrial respiration via an AMPK-dependent signaling mechanism in macrophages, which is not invoked by RvD2.

3.7. 5-Lipoxygenase derived lipid mediators contribute to exercise-induced mitochondrial function via AMPK activation

To assess the *in vivo* relevance of 5-LO derived lipid mediators (e.g., SPMs) in exercise-induced mitochondrial respiration in macrophages, we subjected control and *Alox5*$^{-/-}$ mice to exercise training. After 4 weeks, PM isolated from *Alox5*$^{-/-}$ mice displayed a significant decrease in phosphorylation of AMPK following exercise (Figure 7A). T-distributed stochastic neighbor embedding with FlowSOM clustering analysis identified 4 unique cell populations (e.g., population 1–4), which accounted for greater than 99.0% of total cellular events (Fig. 7B). Populations 1 ($CD45^+F4/80^{high}CD64^{high}$), 3 ($CD45^+F4/80^-CD64^{lo}$), and 4 ($CD45^+F4/80^-CD64^-$) displayed no significant reliance on 5-LO derived lipid mediators for mitochondrial activity following exercise (Figure 7C–E). This contrasted with cells in population 2 ($CD45^+F4/80^{lo}CD64^{lo}$), which displayed a significant reduction in mitochondrial activity with deletion of 5-LO (Fig. 7E). Collectively, these data suggest that *in vivo*, 5-LO derived lipid mediators contribute to AMPK activation and mitochondrial activity in $CD45^+F4/80^{lo}CD64^{lo}$ macrophages following exercise.

4. DISCUSSION

The major findings of this study are that 4 weeks of exercise training in mice significantly enhances the ratio of proresolving lipid mediators (e.g., RvE1 and RvD1) to proinflammatory lipid mediators (e.g., LTB_4). This increased ratio was accompanied by enhanced basal, ATP-linked, and maximal mitochondrial respiratory chain activity in peritoneal macrophages, which suggested a role of SPMs in exercise enhanced macrophage respiration. Data presented herein display that SPMs RvD1, RvD2, RvE1, and MaR1 directly enhance mitochondrial metabolism in peritoneal and bone marrow-derived macrophages. Additionally, the enhancement in macrophage mitochondrial respiration by RvD1 was receptor-dependent, as mice lacking the cognate RvD1 receptor, FPR2, did not display increases in mitochondrial respiration upon RvD1 stimulation. Interestingly, SPM-induced mitochondrial respiration in macrophages is dependent on signaling through the master energy sensor, AMPK, as treatment with Compound C abrogated SPM-induced mitochondrial respiration (e.g., RvD1, RvE1, and MaR1, but not RvD2). This conclusion is supported by our *in vivo* data showing decreased AMPK activation and mitochondrial activity following exercise in macrophages isolated from *Alox5*$^{-/-}$ animals. These data suggest that exercise induced proresolving lipid mediators contribute to enhanced mitochondrial respiration in macrophages via stimulation of AMPK.

Although physical activity imparts its salutary effects by inhibiting the development of chronic inflammation [2,3], the mechanisms by which it may enhance proresolving pathways however remain poorly understood. We previously reported that in a mouse model of aerobic exercise training, physical activity acts as an agonist of inflammation-resolution, by enhancing SPM biosynthesis and macrophage phagocytic capacity [4]. Several studies [24,25,48,51] have established that imbalanced pro-inflammatory-to-proresolving biosynthesis is a defining characteristic of failed resolution and is a contributing factor to the development of chronic inflammatory diseases such as obesity-induced type 2 diabetes and atherosclerosis. This imbalanced production prolongs inflammation and inhibits timely resolution, giving way for the development of chronic inflammation and loss of tissue and organ function [52]. As such, lipid mediators via autocrine/paracrine signaling, play a critical role in maintaining tissue function in both health and disease.

The relationship between metabolism and cellular function in macrophages has been well established. It became increasingly clear during the late 1980s that differential L-Arg catabolism, either via iNOS to produce NO and citrulline (in the case of M1 proinflammatory macrophages), or via Arginase 1 to produce urea, ornithine and polyamines (in the case of M2 anti-inflammatory and proresolving macrophages), was a critical differentiating factor in macrophage activation state [53–56]. Decades later, and although a more complex picture has emerged with numerous metabolic pathways involved, it remains clear that distinct changes in metabolic pathways underlie the immunophenotypic states of macrophages [57,58]. For example, increased reliance on aerobic glycolysis as the primary process for ATP generation, and lower levels of oxidative phosphorylation, along with increased pentose phosphate pathway activity, directly supports the

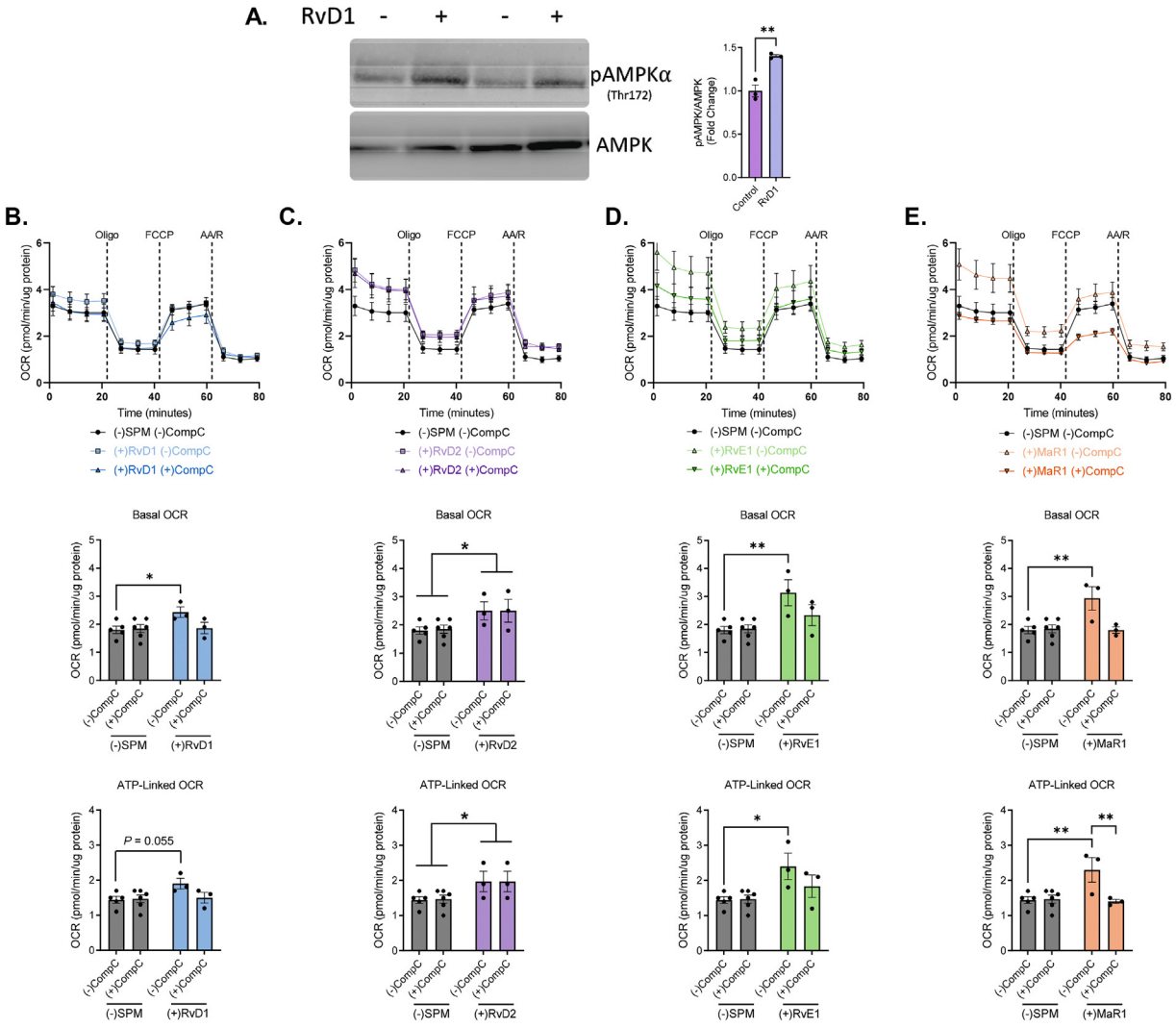

Figure 6: SPMs stimulate AMPKα phosphorylation to enhance mitochondrial metabolism in macrophages. (**A**) Representative immunoblot and quantification (right) of phosphorylated AMPKα (Thr172) and total AMPK in BMDMs treated without or with 1 nM RvD1 for 1h. (**B**–**E**) BMDMs treated without or with 500 nM Compound-C (CompC) and 1 nM of (**B**)RvD1, (**C**) RvD2, (**D**) RvE1, or (**E**) MaR1 for 1h. After treatment, cells were subjected to a mitochondrial stress assay and OCR values assessed (top panels **B**–**E**) and derived mitochondrial respiratory parameters were quantified (below). Data expressed as mean ± SEM; $n = 3$ (**A**) or $n = 3$–6 (**B**–**E**); $^{*}P < 0.05$, $^{**}P < 0.01$; two-tailed Student's *t*-test (a) or Two-way ANOVA with Holm-Šídák post-test (**B**–**E**).

increased biosynthesis of proinflammatory cytokines, inflammatory lipid mediators, and microbicidal superoxide species and citrulline [11,15,23,59]. In contrast, M2 macrophages with an intact and bioenergetically productive TCA cycle rely primarily on oxidative phosphorylation for ATP production. Interestingly, glycolysis, and not necessarily β oxidation, as previously thought, is still required to supply carbon in the form of pyruvate to maintain the TCA cycle. Moreover, this was further illustrated by the fact that blunting of glycolytic flux inhibits IL-4-mediated M2 polarization [7,60]. Despite the increased understanding of the role that cellular metabolism and bioenergetics play in innate immunity, whether and how lipid mediators directly affect macrophage metabolism remains underexplored.

Recent findings, including our work presented here, have provided evidence that changes in macrophage intermediary metabolism upon lipid mediator signaling are involved in eliciting changes in macrophage function. In a study by Fredman et al. [25], mouse BMDMs phagocytosing necroptotic cells (NC), which release a significant amount of prostanoids (namely PGE_2 and TXB_2) relative to apoptotic cells, showed decreased basal and maximal mitochondrial respiration, a phenotype that correlated with increased pro-inflammatory-to-proresolving LM ratio, and diminished phagocytic capacity. Upon treating efferocytic BMDM with the TXA_2 receptor (TP) agonist U-46619, or with NC-conditioned media, a similar phenotype resulted. Moreover, FCCP, a protonophoric uncoupler of mitochondrial respiration that stimulates oxidative phosphorylation, was sufficient to rescue NC-conditioned media treated macrophages. The authors further showed that treatment with RvD1 stimulated fatty acid oxidation as well as basal and ATP-linked respiration in BMDMs. In agreement with our study, Fredman et al. found that RvD1 treatment increased AMPK activation and that inhibition of AMPK kinase activity with Compound C reduced RvD1-stimulated NC uptake and decreased $\Delta\Psi m$. Conversely, treating macrophages with the AMPK activator, AICAR, an adenosine analog that generates an AMPK-activating AMP-mimetic, was able to enhance NC phagocytosis to the same extent as RvD1.

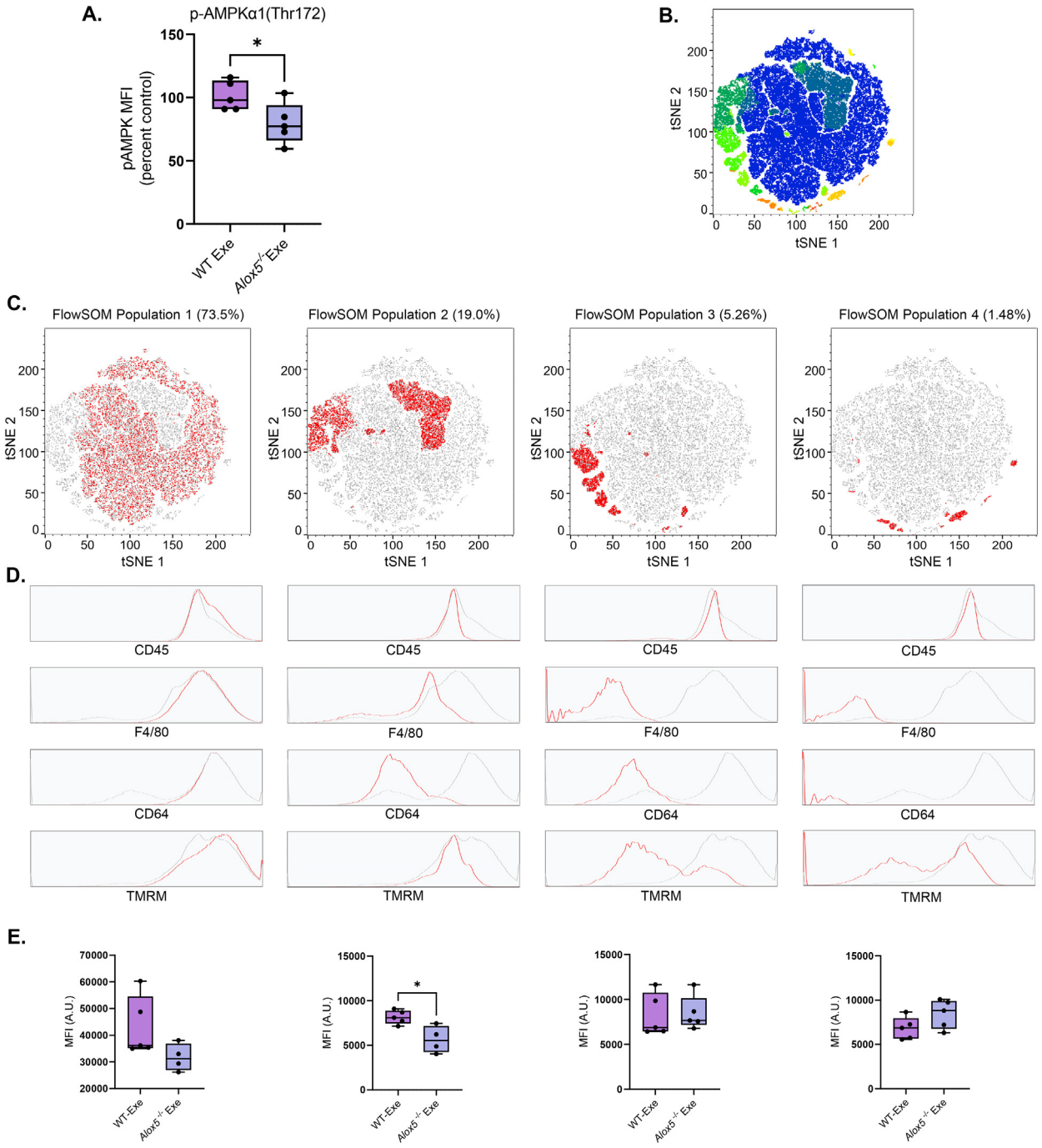

Figure 7: 5-lipoxygenase derived lipid mediators contribute to exercise-induced mitochondrial function via AMPK activation. (**A**) Flow cytometric analysis (MFI) of intracellular AMPKα1(Thr172) phosphorylation in PMs isolated from WT and *Alox5*$^{-/-}$ mice following exercise. (**B**) FlowJo V10.8.1 generated *t*-SNE map (**B,C**) depicted in a 2D dimensionally reduced dataspace showing all events combined from each experimental groups. The color axis overlay in (**B**) depicts metacluster populations identified using FlowSOM, an unbiased machine learning clustering algorithm. (**C**) The percent frequency of each FlowSOM population (highlighted in red) for all samples combined, is denoted atop of the respective *t*-SNE map. (**D**) The fluorescence distribution of each surface marker for the respective FlowSOM metacluster population is shown in red (vs the distribution for all cells shown in grey) in the histogram overlays. (**E**) MFI of TMRM for each FlowSOM metacluster population from WT and *Alox5*$^{-/-}$ mice following exercise. Data expressed as mean ± SEM; $n = 5$ (**A** and **E**); $^{*}P < 0.05$; two-tailed Student's *t*-test.

These findings are congruent with our results showing that SPMs stimulate mitochondrial metabolism in macrophages through activation of AMPK to drive proresolving effector cell functions. Our findings, and the findings by Fredman et al., that SPMs stimulate basal and ATP-linked mitochondrial metabolism suggest that SPMs are stimulating energetically demanding processes and thus increasing ATP demand-processes that likely result in increasing proresolving function such as phagocytic capacity.

In a model of skeletal muscle injury and regeneration, Perretti et al. [49] reported that FPR2 signaling upon Annexin A1 (AnxA1) binding

induced a proresolving phenotype switch crucial for myogenesis. Interestingly, these reparative actions of AnxA1 were dependent upon AMPK signaling as well. Similarly, human PBMC-derived macrophages treated with human recombinant AnxA1 showed phosphorylation of AMPK signaling pathway components CaMK and Acetyl-CoA carboxylase (ACC). The dependence on AMPK signaling in the proresolving phenotypic switch and phagocytic capacity of macrophages in a mouse model of skeletal muscle injury and regeneration was also demonstrated in an earlier study by Mounier et al. [61]. Looking more broadly beyond AMPK involvement in SPM-induced proresolving pathways, two separate studies by Yang et al. [62] and Sag et al. [63], show that exposure to not only canonical M1-polarizing ligands such as LPS, but also to increased FFAs, both *in vivo* and *in vitro*, can increase a pro-inflammatory macrophage phenotype (i.e., increased TNF-α) by decreasing AMPK activation. Similarly, Galic et al. [64] show that BMDMs from mice deficient in the AMPK β1 regulatory subunit display decreased ACC phosphorylation, increased *de novo* fatty acid biosynthesis, and decreased rates of fatty acid oxidation along with a decrease in mitochondrial content. Interestingly, these macrophages display a pro-inflammatory M1 phenotype and have increased pro-inflammatory cytokine production when incubated with saturated fatty acids. Macrophages isolated from AMPK β1-deficient mice also display increased JNK activation concomitant with an increased *iNos*-to-*Arg1* ratio, which are metabolic markers of M1-polarized macrophages. *In vitro* pharmacological activation of AMPK β1 increased ACC phosphorylation resulting in enhanced fatty acid oxidation and a concomitant decrease in inflammatory M1 macrophage phenotype. Conversely, direct pharmacological inhibition of fatty acid oxidation by either the CPT1 inhibitor etomoxir or the complex I inhibitor rotenone resulted in increased M1 macrophage marker expression. Furthermore, bone marrow transplantation from AMPK β1-deficient donors into HFD-fed WT mice, enhanced pro-inflammatory adipose tissue macrophage content, liver insulin resistance, and plasma levels of MCP-1 and TNFα. These data highlight the importance of AMPK signaling in regulating cellular metabolism and macrophage phenotype. Our data extend upon these findings by demonstrating the dependence of AMPK activation in SPM-induced stimulation of mitochondrial activity in macrophages.

In addition to our findings that exercise and SPM-induced AMPK signaling modulates macrophage metabolism, others have also found that catecholamines, which are released during exercise, also induce AMPK activation in adipose tissue, liver, and skeletal muscle of both humans [65] and rats [66—69] in an adrenergic-receptor dependent manner [68,69]. Although, to the best of our knowledge, exercise- and catecholamine-driven AMPK activation and downstream metabolic alterations have not been reported specifically in macrophages, it is interesting to note that in a previous study by our group [4], exercise stimulates SPM biosynthesis in macrophages in an AR-dependent manner. This suggests that the AMPK-dependent enhancements in mitochondrial metabolism shown here could be mediated by exercise-induced catecholamine signaling. The findings presented thus far, coupled with our previous work documenting a role for adrenergic signaling in exercise-enhanced macrophage phagocytosis and resolution of acute inflammation [4], highlight the importance of AMPK-dependent signaling pathways in controlling macrophage metabolism and function.

Taken together, the results of the present study provide strong evidence that proresolving lipid mediators promote mitochondrial respiration in macrophages, which may contribute to the anti-inflammatory effects of exercise. Additionally, our findings suggests that exercise-induced SPM production promotes energetically demanding proresolving processes and concomitant changes in mitochondrial metabolism. These SPM-induced changes in cellular metabolism likely precede stimulation of the proresolving effector functions (e.g., efferocytosis) of macrophages during inflammatory responses. Moreover, anti-inflammatory approaches are associated with increased risk of infection, therefore targeting proresolving pathways to promote mitochondrial metabolism in macrophages provides a distinct therapeutic advantage to prevent the development of chronic inflammatory diseases, similar to the beneficial effects of exercise.

AUTHORS CONTRIBUTIONS

EPC, JH, JZ, NB and PL conducted experiments and analyzed data. EPC and JH wrote the manuscript with input from all the authors. LM and BGH assisted on experimental protocol design and data analysis/interpretation. JH conceived, designed, and supervised the research and writing of the manuscript.

DATA AVAILABILITY

Data will be made available on request.

ACKNOWLEDGEMENTS

The authors thank the University of Louisville Diabetes and Obesity Center Bioanalytical and Flow Cytometry Cores for expert metabolomics and flow cytometry analysis, respectively. Additionally, the authors would like to thank the animal and administrative support staff.

This work was supported in part by National Institutes of Health grants GM127495 (J.H.), HL130174, ES028268, and HL147844 (B.G.H.). The Diabetes and Obesity Center is supported by the National Institutes of Health grant GM127607. Ernesto Pena Calderin is the recipient of an NRSA Ruth L. Kirschstein F31 Fellowship (DK131920). Figure 1A was created with BioRender.com

CONFLICT OF INTEREST

None declared.

APPENDIX A. SUPPLEMENTARY DATA

Supplementary data to this article can be found online at https://doi.org/10.1016/j.molmet.2022.101637.

REFERENCES

[1] Mora S, Cook N, Buring JE, Ridker PM, Lee IM. Physical activity and reduced risk of cardiovascular events: potential mediating mechanisms. Circulation 2007;116(19):2110—8.

[2] Gleeson M, Bishop NC, Stensel DJ, Lindley MR, Mastana SS, Nimmo MA. The anti-inflammatory effects of exercise: mechanisms and implications for the prevention and treatment of disease. Nat Rev Immunol 2011;11(9):607—15.

[3] Nieman DC, Wentz LM. The compelling link between physical activity and the body's defense system. J Sport Health Sci 2019;8(3):201—17.

[4] Zheng J-J, Calderin EP, Hill BG, Bhatnagar A, Hellmann J. Exercise promotes resolution of acute inflammation by catecholamine-mediated stimulation of resolvin D1 biosynthesis. J Immunol 2019;203(11):3013—22.

[5] Farley G, Riggs DW, Bhatnagar A, Hellmann J. Omega-3 polyunsaturated fatty acids modify the inverse association between systemic inflammation and cardiovascular fitness. Clin Nutr 2021;40(6):4097—105.

[6] Van den Bossche J, Baardman J, de Winther MP. Metabolic characterization of polarized M1 and M2 bone marrow-derived macrophages using real-time extracellular flux analysis. JoVE 2015;(105)e53424.

[7] Van den Bossche J, Baardman J, Otto NA, van der Velden S, Neele AE, van den Berg SM, et al. Mitochondrial dysfunction prevents repolarization of inflammatory macrophages. Cell Rep 2016;17(3):684–96.

[8] Vats D, Mukundan L, Odegaard JI, Zhang L, Smith KL, Morel CR, et al. Oxidative metabolism and PGC-1β attenuate macrophage-mediated inflammation. Cell Metabol 2006;4(1):13–24.

[9] Huang SC-C, Smith AM, Everts B, Colonna M, Pearce EL, Schilling JD, et al. Metabolic reprogramming mediated by the mTORC2-IRF4 signaling axis is essential for macrophage alternative activation. Immunity 2016;45(4):817–30.

[10] Tan Z, Xie N, Cui H, Moellering DR, Abraham E, Thannickal VJ, et al. Pyruvate dehydrogenase kinase 1 participates in macrophage polarization via regulating glucose metabolism. J Immunol 2015;194(12):6082–9.

[11] Palsson-McDermott EM, Curtis AM, Goel G, Lauterbach MA, Sheedy FJ, Gleeson LE, et al. Pyruvate kinase M2 regulates Hif-1α activity and IL-1β induction and is a critical determinant of the warburg effect in LPS-activated macrophages. Cell Metabol 2015;21(1):65–80.

[12] Lu B, Nakamura T, Inouye K, Li J, Tang Y, Lundbäck P, et al. Novel role of PKR in inflammasome activation and HMGB1 release. Nature 2012;488(7413):670–4.

[13] Shirai T, Nazarewicz RR, Wallis BB, Yanes RE, Watanabe R, Hilhorst M, et al. The glycolytic enzyme PKM2 bridges metabolic and inflammatory dysfunction in coronary artery disease. J Exp Med 2016;213(3):337–54.

[14] Semba H, Takeda N, Isagawa T, Sugiura Y, Honda K, Wake M, et al. HIF-1α-PDK1 axis-induced active glycolysis plays an essential role in macrophage migratory capacity. Nat Commun 2016;7(1):1–10.

[15] Millet P, Vachharajani V, McPhail L, Yoza B, McCall CE. GAPDH binding to TNF-α mRNA contributes to posttranscriptional repression in monocytes: a novel mechanism of communication between inflammation and metabolism. J Immunol 2016;196(6):2541–51.

[16] Bae S, Kim H, Lee N, Won C, Kim H-R, Hwang Y-I, et al. α-Enolase expressed on the surfaces of monocytes and macrophages induces robust synovial inflammation in rheumatoid arthritis. J Immunol 2012;189(1):365–72.

[17] Jha AK, Huang SC-C, Sergushichev A, Lampropoulou V, Ivanova Y, Loginicheva E, et al. Network integration of parallel metabolic and transcriptional data reveals metabolic modules that regulate macrophage polarization. Immunity 2015;42(3):419–30.

[18] Meiser J, Krämer L, Sapcariu SC, Battello N, Ghelfi J, D'Herouel AF, et al. Pro-inflammatory macrophages sustain pyruvate oxidation through pyruvate dehydrogenase for the synthesis of itaconate and to enable cytokine expression. J Biol Chem 2016;291(8):3932–46.

[19] Infantino V, Convertini P, Cucci L, Panaro MA, Di Noia MA, Calvello R, et al. The mitochondrial citrate carrier: a new player in inflammation. Biochem J 2011;438(3):433–6.

[20] Tannahill G, Curtis A, Adamik J, Palsson-McDermott E, McGettrick A, Goel G, et al. Succinate is an inflammatory signal that induces IL-1β through HIF-1α. Nature 2013;496(7444):238–42.

[21] Lampropoulou V, Sergushichev A, Bambouskova M, Nair S, Vincent EE, Loginicheva E, et al. Itaconate links inhibition of succinate dehydrogenase with macrophage metabolic remodeling and regulation of inflammation. Cell Metabol 2016;24(1):158–66.

[22] Haschemi A, Kosma P, Gille L, Evans CR, Burant CF, Starkl P, et al. The sedoheptulose kinase CARKL directs macrophage polarization through control of glucose metabolism. Cell Metabol 2012;15(6):813–26.

[23] Mills EL, Kelly B, Logan A, Costa AS, Varma M, Bryant CE, et al. Succinate dehydrogenase supports metabolic repurposing of mitochondria to drive inflammatory macrophages. Cell 2016;167(2):457–70. e13.

[24] Fredman G, Hellmann J, Proto JD, Kuriakose G, Colas RA, Dorweiler B, et al. An imbalance between specialized pro-resolving lipid mediators and pro-inflammatory leukotrienes promotes instability of atherosclerotic plaques. Nat Commun 2016;7(1):1–11.

[25] Hosseini Z, Marinello M, Decker C, Sansbury BE, Sadhu S, Gerlach BD, et al. Resolvin D1 enhances necroptotic cell clearance through promoting macrophage fatty acid oxidation and oxidative phosphorylation. Arterioscler Thromb Vasc Biol 2021;41(3):1062–75.

[26] Viola JR, Lemnitzer P, Jansen Y, Csaba G, Winter C, Neideck C, et al. Resolving lipid mediators maresin 1 and resolvin D2 prevent atheroprogression in mice. Circ Res 2016;119(9):1030–8.

[27] Serhan CN, Petasis NA. Resolvins and protectins in inflammation resolution. Chem Rev 2011;111(10):5922–43.

[28] Serhan CN, Chiang N, Van Dyke TE. Resolving inflammation: dual anti-inflammatory and pro-resolution lipid mediators. Nat Rev Immunol 2008;8(5):349–61.

[29] Dyall SC, Balas L, Bazan NG, Brenna JT, Chiang N, da Costa Souza F, et al. Polyunsaturated fatty acids and fatty acid-derived lipid mediators: recent advances in the understanding of their biosynthesis, structures, and functions. Prog Lipid Res 2022101165.

[30] Belkina AC, Ciccolella CO, Anno R, Halpert R, Spidlen J, Snyder-Cappione JE. Automated optimized parameters for T-distributed stochastic neighbor embedding improve visualization and analysis of large datasets. Nat Commun 2019;10(1):1–12.

[31] Van Gassen S, Callebaut B, Van Helden MJ, Lambrecht BN, Demeester P, Dhaene T, et al. FlowSOM: using self-organizing maps for visualization and interpretation of cytometry data. Cytometry, Part A 2015;87(7):636–45.

[32] Kregel KC, Allen DL, Booth FW, Fleshner MR, Henriksen EJ, Musch T, et al. Resource book for the design of animal exercise protocols. American Physiological Society; 2006. p. 152.

[33] Powell WS, Rokach J. The eosinophil chemoattractant 5-oxo-ETE and the OXE receptor. Prog Lipid Res 2013;52(4):651–65.

[34] O'Flaherty JT, Thomas MJ. Effect of 15-lipoxygenase-derived arachidonate metabolites on human neutrophil degranulation. Prostaglandins Leukot Med 1985;17(2):199–212.

[35] Morita E, Schröder J, Christophers E. Identification of a novel and highly potent eosinophil chemotactic lipid in human eosinophils treated with arachidonic acid. J Immunol 1990;144(5):1893–900.

[36] Sander J, Schmidt SV, Cirovic B, McGovern N, Papantonopoulou O, Hardt A-L, et al. Cellular differentiation of human monocytes is regulated by time-dependent interleukin-4 signaling and the transcriptional regulator NCOR2. Immunity 2017;47(6):1051–66. e12.

[37] Tarique AA, Logan J, Thomas E, Holt PG, Sly PD, Fantino E. Phenotypic, functional, and plasticity features of classical and alternatively activated human macrophages. Am J Respir Cell Mol Biol 2015;53(5):676–88.

[38] Beyer M, Mallmann MR, Xue J, Staratschek-Jox A, Vorholt D, Krebs W, et al. High-resolution transcriptome of human macrophages. 2012.

[39] Lescoat A, Ballerie A, Augagneur Y, Morzadec C, Vernhet L, Fardel O, et al. Distinct properties of human M-CSF and GM-CSF monocyte-derived macrophages to simulate pathological lung conditions in vitro: application to systemic and inflammatory disorders with pulmonary involvement. Int J Mol Sci 2018;19(3):894.

[40] Ohradanova-Repic A, Machacek C, Fischer MB, Stockinger H. Differentiation of human monocytes and derived subsets of macrophages and dendritic cells by the HLDA10 monoclonal antibody panel. Clinical & Translational Immunology 2016;5(1):e55.

[41] Namgaladze D, Brüne B. Fatty acid oxidation is dispensable for human macrophage IL-4-induced polarization. Biochim Biophys Acta, Mol Cell Biol Lipids 2014;1841(9):1329–35.

[42] Perry SW, Norman JP, Barbieri J, Brown EB, Gelbard HA. Mitochondrial membrane potential probes and the proton gradient: a practical usage guide. Biotechniques 2011;50(2):98–115.

[43] Nicholls DG. Mitochondrial membrane potential and aging. Aging Cell 2004;3(1):35–40.

[44] Salabei JK, Gibb AA, Hill BG. Comprehensive measurement of respiratory activity in permeabilized cells using extracellular flux analysis. Nat Protoc 2014;9(2):421–38.
[45] Hill BG, Benavides GA, Lancaster JR, Ballinger S, Dell'Italia L, Zhang J, et al. Integration of cellular bioenergetics with mitochondrial quality control and autophagy. Biol Chem 2012;393(12):1485–512.
[46] Garedew A, Henderson SO, Moncada S. Activated macrophages utilize glycolytic ATP to maintain mitochondrial membrane potential and prevent apoptotic cell death. Cell Death Differ 2010;17(10):1540–50.
[47] Datta G, Kramer PA, Johnson MS, Sawada H, Smythies LE, Crossman DK, et al. Bioenergetic programming of macrophages by the apolipoprotein AI mimetic peptide 4F. Biochem J 2015;467(3):517–27.
[48] Hellmann J, Tang Y, Kosuri M, Bhatnagar A, Spite M. Resolvin D1 decreases adipose tissue macrophage accumulation and improves insulin sensitivity in obese-diabetic mice. FASEB J 2011;25(7):2399–407.
[49] McArthur S, Juban G, Gobbetti T, Desgeorges T, Theret M, Gondin J, et al. Annexin A1 drives macrophage skewing to accelerate muscle regeneration through AMPK activation. J Clin Invest 2020;130(3):1156–67.
[50] Chiang N, Sakuma M, Rodriguez AR, Spur BW, Irimia D, Serhan CN. Resolvin T-series reduce neutrophil extracellular traps. Blood, The Journal of the American Society of Hematology 2022;139(8):1222–33.
[51] Spite M, Hellmann J, Tang Y, Mathis SP, Kosuri M, Bhatnagar A, et al. Deficiency of the leukotriene B4 receptor, BLT-1, protects against systemic insulin resistance in diet-induced obesity. J Immunol 2011;187(4):1942–9.
[52] Rius B, López-Vicario C, González-Périz A, Morán-Salvador E, García-Alonso V, Clària J, et al. Resolution of inflammation in obesity-induced liver disease. Front Immunol 2012;3:257.
[53] Stuehr DJ, Marletta MA. Mammalian nitrate biosynthesis: mouse macrophages produce nitrite and nitrate in response to Escherichia coli lipopolysaccharide. Proc Natl Acad Sci USA 1985;82(22):7738–42.
[54] Iyengar R, Stuehr DJ, Marletta MA. Macrophage synthesis of nitrite, nitrate, and N-nitrosamines: precursors and role of the respiratory burst. Proc Natl Acad Sci USA 1987;84(18):6369–73.
[55] Hibbs J, Vavrin Z, Taintor R. L-arginine is required for expression of the activated macrophage effector mechanism causing selective metabolic inhibition in target cells. J Immunol 1987;138(2):550–65.
[56] Granger DL, Hibbs J, Perfect JR, Durack DT. Specific amino acid (L-arginine) requirement for the microbiostatic activity of murine macrophages. J Clin Invest 1988;81(4):1129–36.
[57] Van den Bossche J, O'Neill LA, Menon D. Macrophage immunometabolism: where are we (going)? Trends Immunol 2017;38(6):395–406.
[58] Galván-Peña S, O'Neill LA. Metabolic reprograming in macrophage polarization. Front Immunol 2014;5:420.
[59] Jiang H, Shi H, Sun M, Wang Y, Meng Q, Guo P, et al. PFKFB3-driven macrophage glycolytic metabolism is a crucial component of innate antiviral defense. J Immunol 2016;197(7):2880–90.
[60] Covarrubias AJ, Aksoylar HI, Yu J, Snyder NW, Worth AJ, Iyer SS, et al. Akt-mTORC1 signaling regulates Acly to integrate metabolic input to control of macrophage activation. Elife 2016;5e11612.
[61] Mounier R, Théret M, Arnold L, Cuvellier S, Bultot L, Göransson O, et al. AMPKα1 regulates macrophage skewing at the time of resolution of inflammation during skeletal muscle regeneration. Cell Metabol 2013;18(2):251–64.
[62] Yang Z, Kahn BB, Shi H, Xue B-z. Macrophage α1 AMP-activated protein kinase (α1AMPK) antagonizes fatty acid-induced inflammation through SIRT1. J Biol Chem 2010;285(25):19051–9.
[63] Sag D, Carling D, Stout RD, Suttles J. Adenosine 5′-monophosphate-activated protein kinase promotes macrophage polarization to an anti-inflammatory functional phenotype. J Immunol 2008;181(12):8633–41.
[64] Galic S, Fullerton MD, Schertzer JD, Sikkema S, Marcinko K, Walkley CR, et al. Hematopoietic AMPK β1 reduces mouse adipose tissue macrophage inflammation and insulin resistance in obesity. J Clin Invest 2011;121(12):4903–15.
[65] Watt MJ, Holmes AG, Pinnamaneni SK, Garnham AP, Steinberg GR, Kemp BE, et al. Regulation of HSL serine phosphorylation in skeletal muscle and adipose tissue. Am J Physiol Endocrinol Metab 2006;290(3):E500–8.
[66] Koh H-J, Hirshman MF, He H, Li Y, Manabe Y, Balschi JA, et al. Adrenaline is a critical mediator of acute exercise-induced AMP-activated protein kinase activation in adipocytes. Biochem J 2007;403(3):473–81.
[67] Ruderman N, Park H, Kaushik V, Dean D, Constant S, Prentki M, et al. AMPK as a metabolic switch in rat muscle, liver and adipose tissue after exercise. Acta Physiol Scand 2003;178(4):435–42.
[68] Hutchinson DS, Bengtsson T. AMP-activated protein kinase activation by adrenoceptors in L6 skeletal muscle cells: mediation by α1-adrenoceptors causing glucose uptake. Diabetes 2006;55(3):682–90.
[69] Hutchinson DS, Chernogubova E, Dallner OS, Cannon B, Bengtsson T. β-Adrenoceptors, but not α-adrenoceptors, stimulate AMP-activated protein kinase in brown adipocytes independently of uncoupling protein-1. Diabetologia 2005;48(11):2386–95.

